Christopher Strobl BSc

Analyses of displacement vectors in the „Haltestelle Eichberg“ fault zone at the Semmering Base Tunnel

Master’s Thesis

Submitted in fulfilment of the requirements for the degree of

Diplom-Ingenieur / Diplom-Ingenieurin

Master’s programme Civil Engineering, Geotechnics and Hydraulics

at

Graz University of Technology

Supervisor:
O.Univ.-Prof. Dipl.-Ing. Dr.mont. Wulf Schubert

Institute of Rock Mechanics and Tunnelling
Graz University of Technology

Reviewers:
Dipl.-Ing. Alexander Kluckner
Dipl.-Ing. Gerold Lenz

Graz, March 2018

EIDESSTATTLICHE ERKLÄRUNG
AFFIDAVIT

Ich erkläre an Eides statt, dass ich die vorliegende Arbeit selbstständig verfasst, andere als die angegebenen Quellen/Hilfsmittel nicht benutzt, und die den benutzten Quellen wörtlich und inhaltlich entnommenen Stellen als solche kenntlich gemacht habe. Das in TUGRAZonline hochgeladene Textdokument ist mit der vorliegenden Masterarbeit identisch.

I declare that I have authored this thesis independently, that I have not used other than the declared sources/resources, and that I have explicitly marked all material which has been quoted either literally or by content from the used sources. The text document uploaded to TUGRAZonline is identical to the present master‘s thesis.

Datum / Date	Unterschrift / Signature

Acknowledgements

Thank you, to all the members of the Institute of Rock Mechanics and Tunnelling under the lead of Professor Wulf Schubert for the constant support, to the Austrian Federal Railways (ÖBB) for providing the essential data, but most of all to my advisers Dipl.-Ing. Alexander Kluckner and Dip.-Ing. Gerold Lenz from the iC group, for their help and for always lending me an open ear for discussion.

Special gratitude belongs to my family and friends for providing me advice and encouragement for as long as I can remember.

Abstract

To understand the behaviour of the system formed by the rock mass and the tunnel structure, one must try to relate the observed phenomena to potential physical mechanisms mainly determined by the architecture of the rock mass. In this work it was attempted to identify such mechanisms for the observations made tunnelling through the "Haltestelle Eichberg" fault zone at construction lot SBT1.1, track 1, of the Semmering Base Tunnel.

State-of-the-art monitoring data interpretation techniques combined with simple numerical calculations have been used to link the system behaviour to the geological conditions. Eventually, reasonable explanations were found for selected phenomena. Locally changing rock mass characteristics mapped at the face could be successfully linked to trends of displacement vector orientations. Results of numerical calculations helped to confirm formulated hypotheses.

It could be shown that a detailed measurement data interpretation in combination with comprehensive geological information and rather simple numerical models allows to link the behaviour of underground structures in even very complex geological conditions to basic mechanisms.

Kurzfassung

Um das Verhalten des aus dem Gebirge und der Tunnelschale gebildeten Systems zu verstehen, ist es von entscheidender Bedeutung, die möglichen, zugrundeliegenden Mechanismen der beobachteten Phänomene in die Betrachtung miteinzubeziehen. In dieser Arbeit wurden solche physikalischen Mechanismen, bestimmt durch die Architektur des Gebirges, für die Beobachtungen beim Durchörtern der Störungszone „Haltestelle Eichberg“ am Baulos SBT1.1, Gleis1, des Semmering-Basistunnels, identifiziert.

Um das Systemverhalten mit der angetroffenen Geologie zu verknüpfen, wurden aktuelle Messdateninterpretationsmethoden verbunden mit einfachen numerischen Modellen verwendet. Schlussendlich konnten somit plausible Erklärungen für ausgewählte Phänomene gefunden werden. Lokale Änderungen der Gebirgssteifigkeit konnten erfolgreich mit Trends der Verschiebungsvektororientierung in Verbindung gebracht werden. Mit Hilfe der numerischen Analysen konnten zuvor aufgestellten Hypothesen bestätigt werden.

Es konnte gezeigt werden, dass es eine detaillierte Messdateninterpretation kombiniert mit umfassender geologischer Information und einfach gehaltenen numerischen Modellen ermöglicht, das Systemverhalten von Untertagebauten auch in komplexen, geologischen Umständen durch simple Mechanismen zu erklären.

Table of contents

List of figures

List of tables

Abbreviations

RMT.....rock mass type

Dip.....dip angle

DipDir .....dip direction

Fl .....foliation

Fz .....fault zone

Fa .....fault

TA.....tunnel axis

LDP .....longitudinal displacement profile

V.....vertical displacements

H.....horizontal displacements

S.....settlements

MS.....monitoring section

FE.....finite element

E.....young´s modulus

φ .....friction angle

c .....cohesion

σ_c .....uniaxial compressive strength

1 Introduction

1.1 Objective

During the construction of the lot SBT1.1 “Tunnel Gloggnitz” of the Semmering Base Tunnel characteristic deformation patterns occurred in the area of the “Haltestelle Eichberg” fault system. The analysis and the investigation of these deformations served as the basis for this work.

It was of special interest to identify and investigate the underlying mechanisms that ultimately provoked the measured displacements. This includes the identification of mechanical significant geological features and an assessment of how these features influence the deformations.

1.2 Methodology

At first, a general overview of the encountered geological conditions in the area of the “Haltestelle Eichberg” fault system was established. This includes a schematic explanation of the geological features including a parametric description of the encountered rock mass types.

Then, the geological conditions were assessed in further detail and were separated into sections that show similar attributes. Stereographic projection plots of mapped discontinuities were generated throughout the entire area of interest and depicted together with sketches of the tunnel faces.

Further, distinct phenomena were identified and systematically investigated. Special attention was given to the vector orientation of the displacement vectors and their magnitude.

The first step was to compare the occurring phenomena to findings of publications and to test their applicability. In case no explanation could be directly derived, further investigations had to be conducted, beginning with the stating of working-hypothesis regarding a possible cause-effect relation between encountered geological features and the observed behaviour. Later trying to either verify or disprove these hypothesis until the most probable cause-effect relation could be determined.

2 Geological Situation

The “Haltestelle Eichberg Seitenverschiebung” is a prominent fault zone located below the “Eichberg” train station of the current Semmering railway. The overburden above the crown is between 130m and 140m in this area.

The rock mass consists of phyllites and schist of the “Silbersberggruppe” partially rich in quartz. Because of intensive tectonic overprint along the fault system, the rocks are sericitized, sheared and exist mostly as fault material. The fault system strikes in a west-east direction and dips steeply towards north.

The foliation dips either steeply in direction North or steeply in direction South. The shear bands cross the tunnel axis in an angle between 25° to 50° and primarily dip against the direction of excavation.

Typical for the fault system is a high degree of fracturing and the destrengthening of the phyllite and schist to mainly fine grained cataclastic rock. Inside the cataclastic stratus, shear bodies of quartzite and dolomite in a *cm – dm* dimension are interbedded. Fault zones with a high cataclastic proportion reach thicknesses in the lower 10 - meter range. Fault zones with mediocre cataclastic proportions carry tectonically spared areas, where the structural fabric of the intact rock is preserved, but the strength is already considerably decreased in comparison.

By the presence of swelling clay minerals, a swelling potential inside the fault material as well as in the spared areas exists.

2.1 Controlling Rock Mass Types

For the corresponding rock mass section, different rock mass types were distinguished in the geo-mechanical design. The major rock mass types (RMT) encountered in the area of the “Haltestell Eichberg” fault zone are RMT 2a, RMT 2b-2, RMT 8c and RMT 8f.

2.1.1 RMT 2a

The rock mass type represents a highly fractured and sheared phyllite. It is strongly anisotopic and under load it tends to break along the foliation planes.

Table 2.1: Parameters RMT 2a

Parameter	Unit	Intact Rock	Rock Mass
σ_c	[MPa]	20 - 50	1 - 4
c	[MPa]	6 - 15	0.5 - 1.5
φ	[°]	23 - 24	18 - 24
E	[GPa]	20 - 40	1 - 3.5

Discontinuities are sheared parallel to the geomechanically potent foliation and mostly tectonically stressed. The majority of the formed joints and slickensides contain a clayey-sericitic filling.

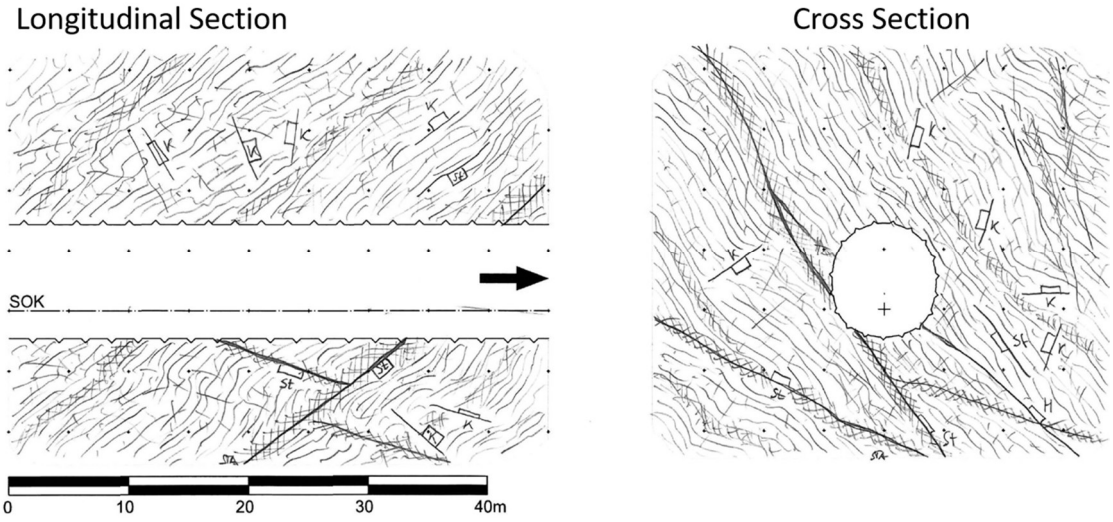

Figure 2.1: Schematic sketch RMT 2a strata *(1)*

2.1.2 RMT 2b-2

The RMT 2b-2 describes a highly fractured schist partially subjected to tectonic shearing. In intact state, the rock can be described as medium to strongly anisotropic with primarily mediocre strength attributes.

Table 2.2: Parameters RMT 2b-2

Parameter	Unit	Intact Rock	Rock Mass
σ_c	[MPa]	20 - 60	2.5 - 7
c	[MPa]	5 - 15	1 - 2
φ	[°]	29 - 37	21 - 28
E	[GPa]	25 - 45	1.5 – 5

The discontinuities in the RMT 2b-2 are primarily strongly tectonically stressed, highly fractured and partially sheared parallel to foliation. The foliation has a spacing of 2 – 6 *cm* with locally occurring deviations. In heavily distorted areas, cataclastic rock in *cm* – *dm* range is observed.

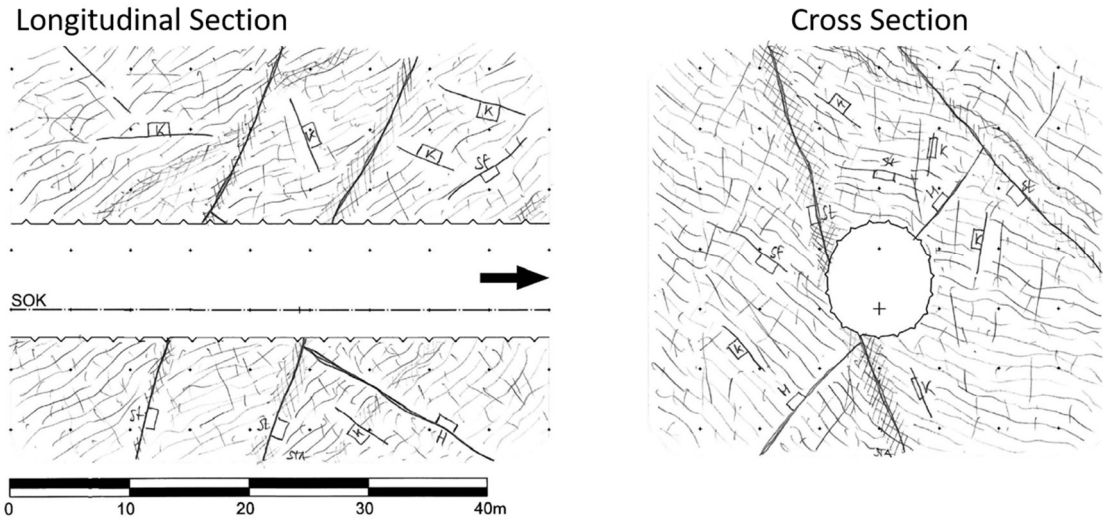

Figure 2.2: Schematic sketch RMT 2b-2 strata *(1)*

2.1.3 RMT 8c

This RMT describes a fault zone material consisting of cataclastic rock formed from schistose and phyllitic rock, as well as of spared areas.

Table 2.3: Parameters RMT 8c

Parameter	Unit	Intact Rock	Rock Mass
σ_c	[MPa]	-	0.05 - 1
c	[MPa]	-	0.06 - 0.8
φ	[°]	-	23 - 27
E	[GPa]	-	0.4 - 10

The fault zone material is dominated by cataclastic rock rich on sheet silicate and primarily shows a silty-sandy-gravely grain size distribution. The proportion of cataclastic rock in the rock mass is in a range of about 30% – 70%.
The tectonically spared areas consist of mostly sheared but in the structure competent rock, that appears between the fault zone material. Frequently, smooth to polished slickensides are encountered.
This RMT occurs as a strongly tectonically stressed rock mass in a lesser fractured rock mass, or in the outskirts of large fault zones with a high proportion of cataclastic rock and spared areas with a high degree of fracturing.

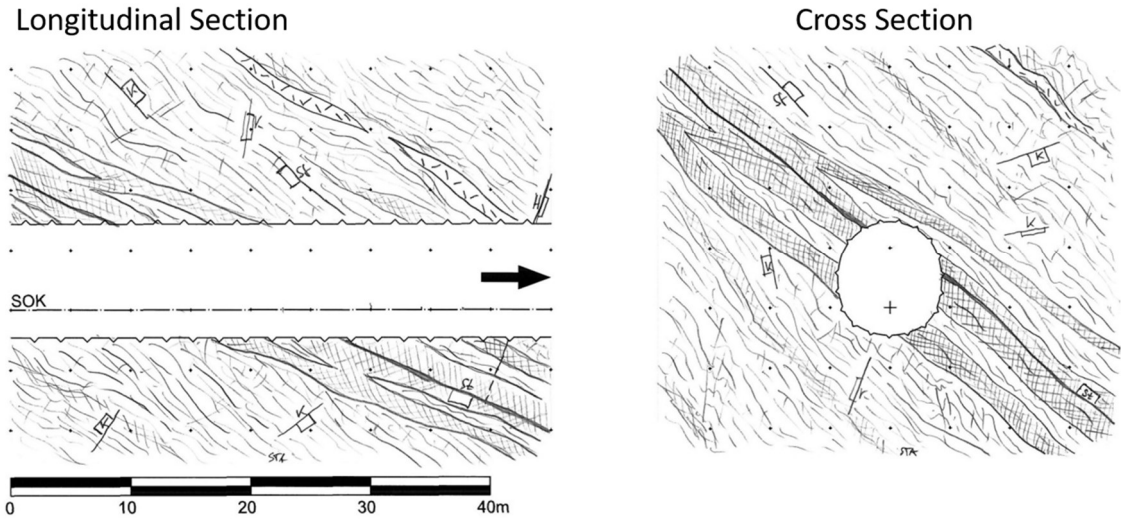

Figure 2.3: Schematic sketch RMT 8c strata *(1)*

- RMT 8f

In contrast to RMT 8c, the cataclastic rock in RMT 8f has dominating silt and a minor sandy-gravelly proportion. Again, the source rocks for this RMT are sericite phyllite and schist.

Table 2.4: Parameters RMT 8f

Parameter	Unit	Intact Rock	Rock Mass
σ_c	[MPa]	-	0.05 - 1
c	[MPa]	-	0.1 - 0.15
φ	[°]	-	23 - 25
E	[GPa]	-	0.17-0,37 (at σ_1 = 5 MPa)

This RMT occurs in locally major fault zones with an extent of m to 10 x m dimensions and is frequently accompanied by zones of lesser cataclastic components like described here by RMT 8c.

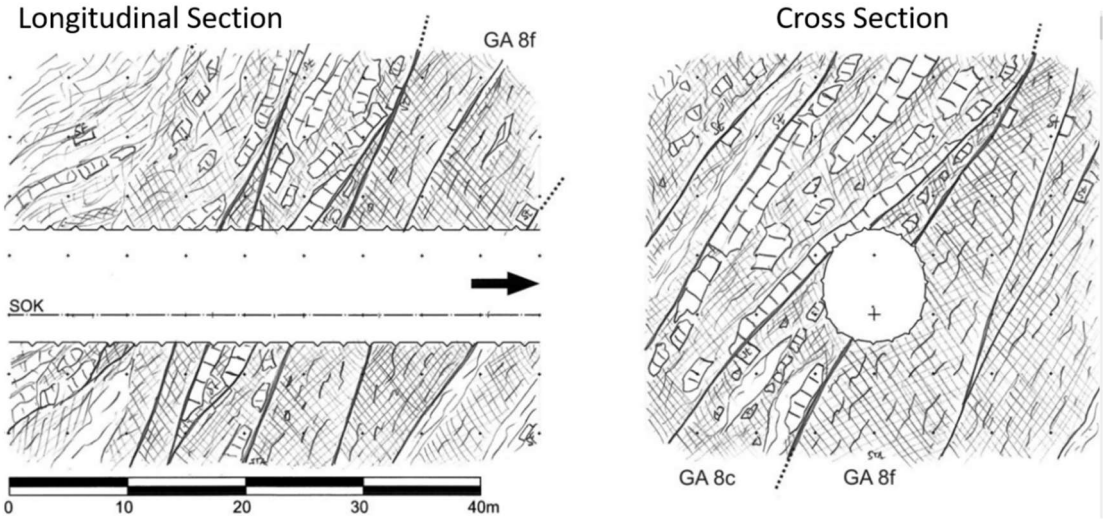

Figure 2.4: Schematic sketch RMT 8c/8f strata *(1)*

2.2 Detailed Assessment

With the help of intern planning documents, the previously mentioned RMTs are put into context of the geological situation distributed along the tunnel axis at the “Haltestelle Eichberg Seitenverschiebung”.

Track 1 chainage 1330m - 1352m RMT 8c Fault zone:

In this section, very frequent changes between disintegrated zones with cataclastic overprint, shear zones with a high proportion of cataclastic rock and spared areas occur. The cataclastic rock has a sandy gravelly grain size distribution, consisting of disintegrated schist with interbedded sericite-phyllite and quartz-phyllite. The stratus is crumbly and sometimes destrengthened. Due to the cataclastic overprint, the foliation is sometimes hard to identify. In Figure 2.5 the encountered foliation is depicted (green) together with the tunnel axis (orange).

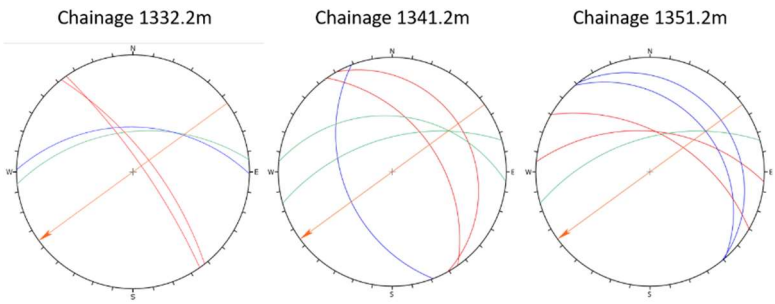

Figure 2.5 Discontinuities chainage 1330m - 1352 m (Fl: green, SL: red, Fa: blue)

Multiple faults and slickensides with clayey filling disturb the rock mass in this area.

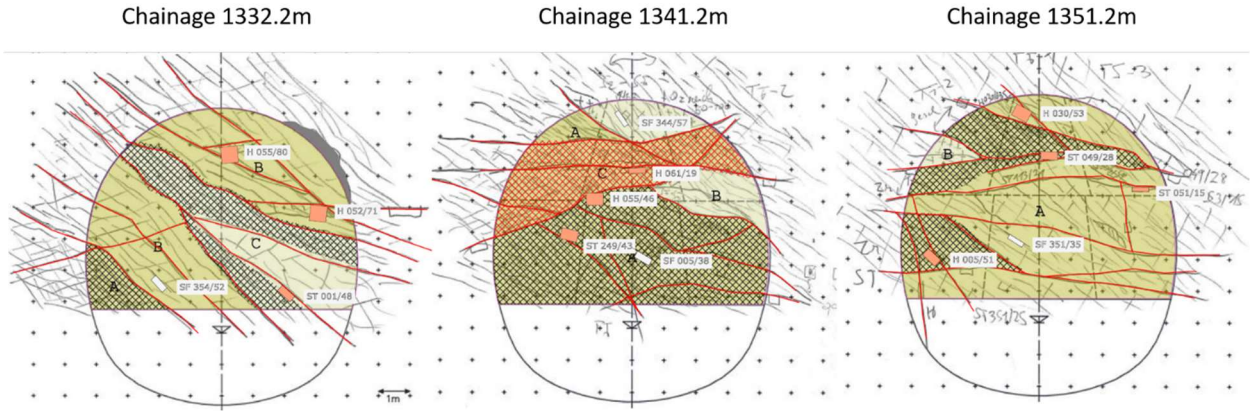

Figure 2.6: Face documentation chainage 1330m -1352m *(2)*

<u>Track 1 chainage 1352m – 1372m RMT 2b-2 spared area:</u>

The rock mass is partly highly fractured and cataclasticly overprinted alongside discontinuities. The foliation dips flatly to slightly steeply towards north, as described above, and is geo-mechanically active. Multiple faults and slickensides dip steeply against the direction of drive.

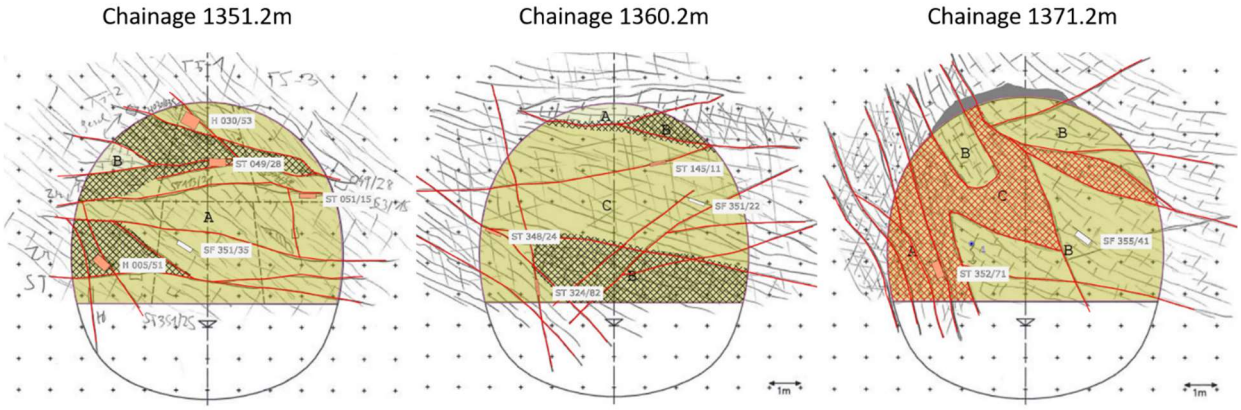

Figure 2.7 Face documentation chainage 1350m - 1370m *(2)*

Track 1 chainage 1372m -1452m RMT 8c Fault zone:

This is where the first core zone of the “Haltestelle Eichberg Seitenverschiebung” fault system is located. The rock mass is similar to the one observed at chainage 1330m - 1352m, but the cataclastic rock has a rather silty - sandy to clayey - silty characteristics here. The fault zone is dipping steeply towards NNW, with an acute angle to the tunnel axis, entering the cavity from the left. Due to the high content of fine grained material, swelling potential must be expected.

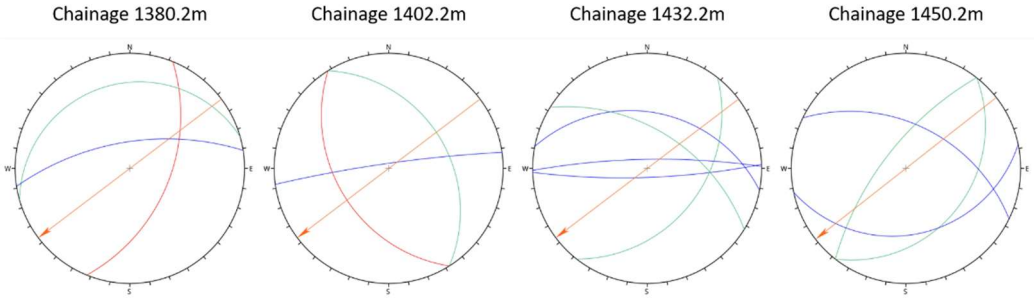

Figure 2.8: Discontinuities chainage 1372m - 1452m (Fl: green, SL: red, Fa: blue)

The foliation in this section turns from a N-W direction towards a S-E direction at the end. Also, after chainage 1440m an additional foliation is identified.

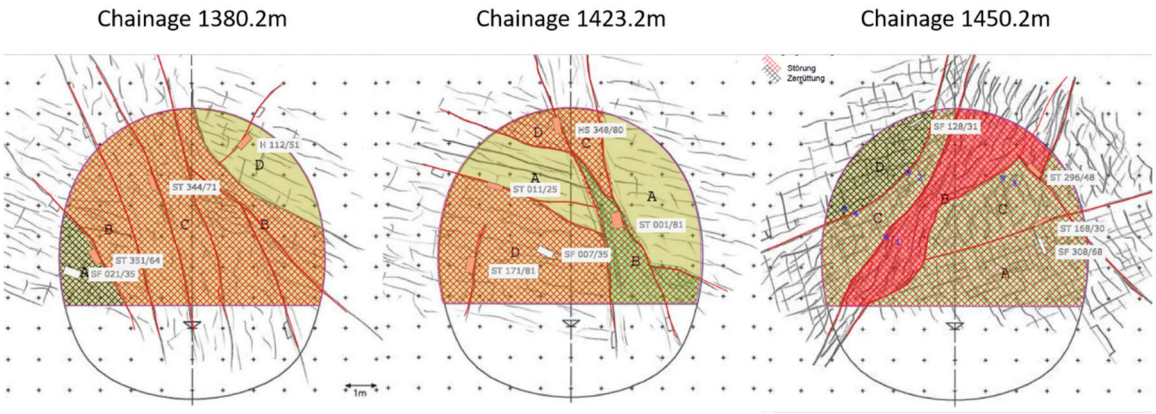

Figure 2.9: Face documentation chainage 1372m-1452m *(2)*

Track 1 chainage 1452m -1494m RMT 2b-2 spared areas:

The biggest difference in this section compared with the spared area between chainage 1352m and 1372m is that the foliation shifts from dipping mainly towards north to now dipping face outward towards a N-E to S-E direction.

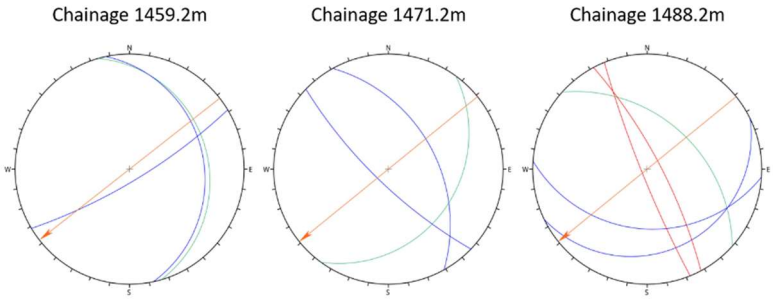

Figure 2.10: Discontinuities chainage 1452m - 1494m (Fl: green, SL: red, Fa: blue)

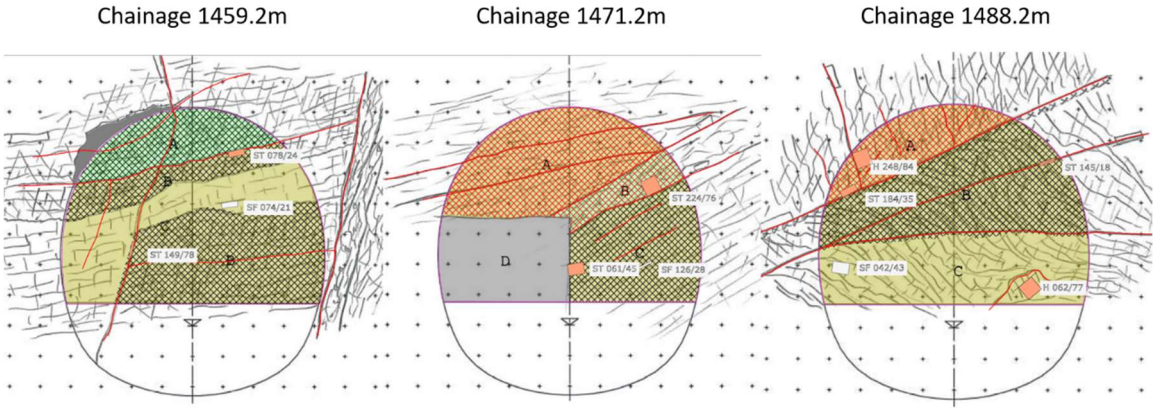

Figure 2.11: Face documentation chainage 1452m – 1494m *(2)*

Track 1 chainage 1494 - 1558 RMT 8c Fault Zone:

Here, a further core zone of the “Haltestelle Eichberg Seitenverschiebung” intersects the tunnel axis. In contrast to the previous core zone, a sandy - gravelly grain size distribution of the cataclastic rock is dominant. Locally minor silty - clayey shear bands disturb the stratus. Interbedded, areas with characteristics of RMT 2b-2 and RMT 2a are found

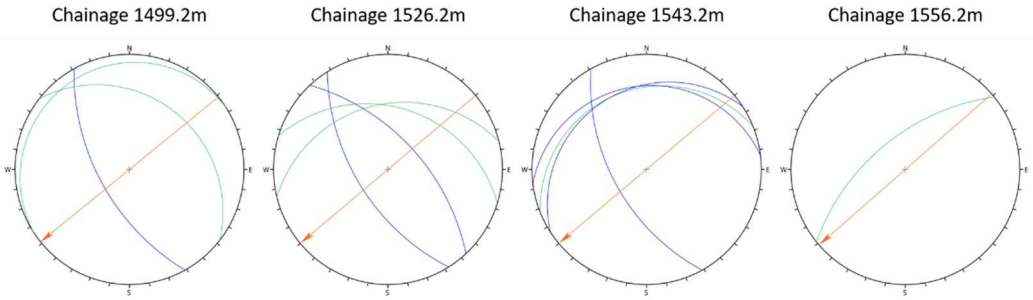

Figure 2.12: Discontinuities chainage 1494m - 1558m (Fl: green, SL: red, Fa: blue)

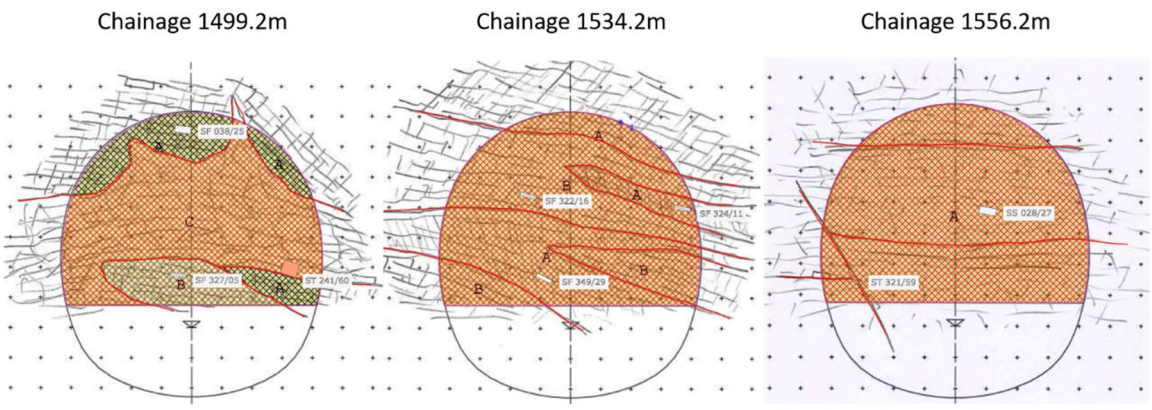

Figure 2.13: Face documentation chainage 1494m - 1558m *(2)*

Track 1 chainage 1558 - 1641: RMT 2a Tectonically disintegrated Phyllite and Chlorite-Phyllite

The stratus consists of very tightly foliated rock, sheared along the foliation planes and partially cataclasticly overprinted. Towards the end of the section, the tectonic overprinting diminishes. A higher movability and a higher potential of rock fall occurs along steep slickensides dipping against direction of drive. The foliation is folded wavy and is continuously steepening until it reaches a dipping angle of 70° towards the end of the section.

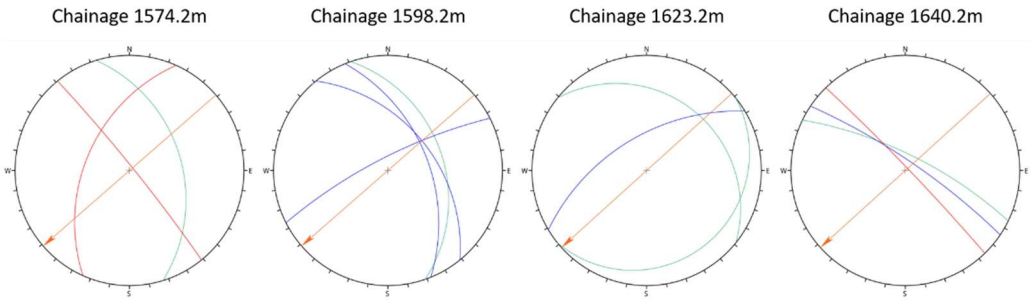

Figure 2.14: Discontinuities chainage 1558m - 1641m (Fl: green, SL: red, Fa: blue)

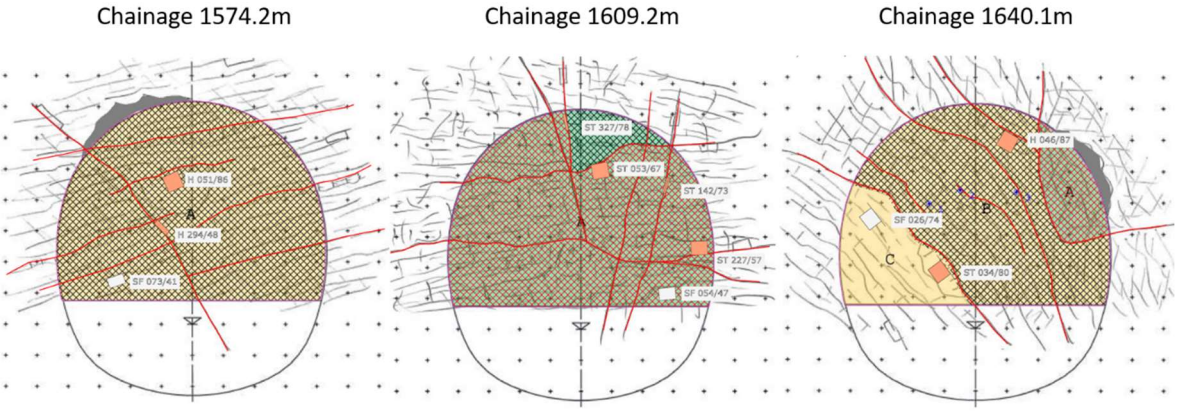

Figure 2.15: Face documentation chainage 1558m - 1641m *(2)*

Track 1 chainage 1641 - 1700: RMT 2b-2 Series of quarzitic and phyllitic schist

This area is tectonically heavily stressed and fractured. Strength attributes are varying according to the lithology, from crumbly to moderately hard. In disintegrated areas as well as in very tightly foliated areas, the strength can significantly decrease. Overall the stratus is thin bedded to thin platy, in phyllitic areas also leafy foliated. The foliation is dipping steeply face outward and is geomechanically very potent due to silty filling.

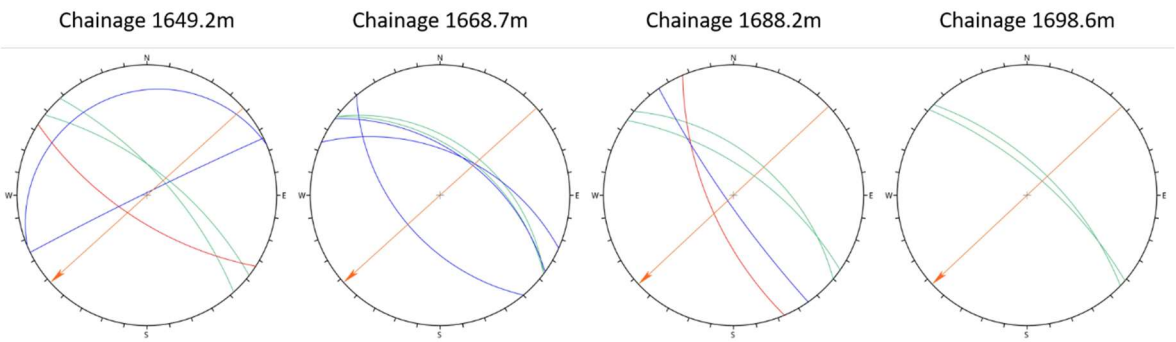

Figure 2.16: Discontinuities chainage 1641m - 1700m (Fl: green, SL: red, Fa: blue)

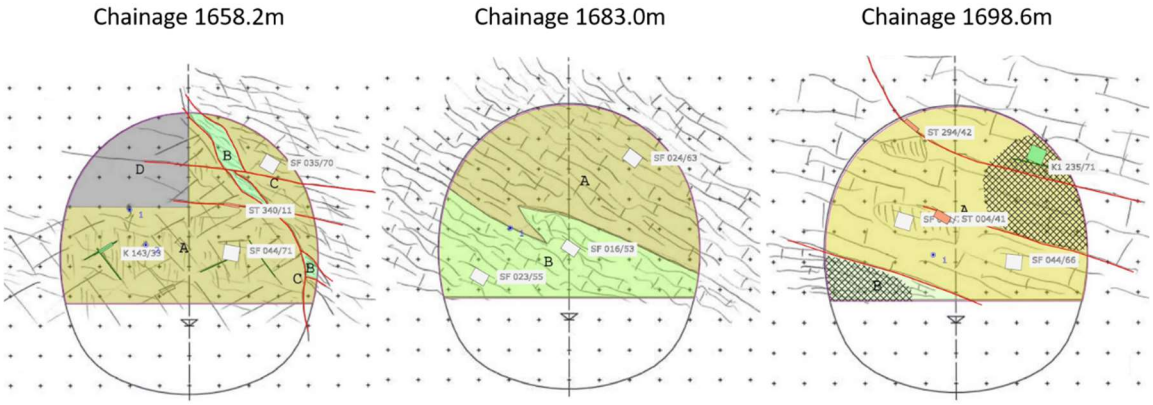

Figure 2.17: Face documentation chainage 1641m - 1700m *(2)*

3 Displacement Data

At the Semmering Base Tunnel, an absolute 3D displacement monitoring system has been established to observe of the system behaviour. The measurement is conducted via a total station, measuring angle and distance to prism targets installed at the shotcrete liner.

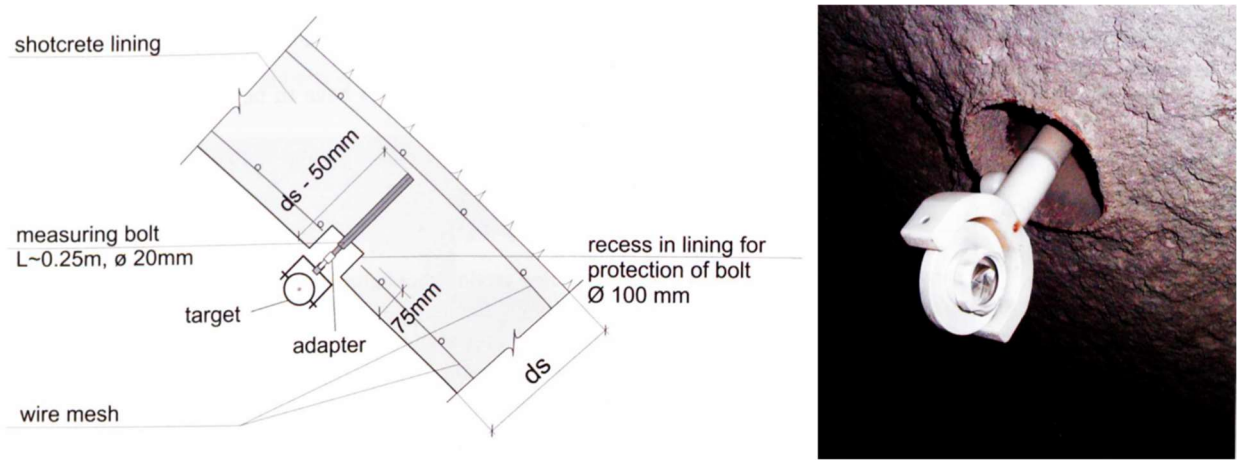

Figure 3.1: Sketch of target installation (left), installed prism target (right) *(3)*

With the 3D displacement monitoring, the horizontal, the vertical and the longitudinal movement of the shotcrete liner can be observed. An evaluation of relative and absolute movements with a precision of ± 1 mm is possible with this method.

The measurements were taken using the free stationing method as schematically depicted in Figure 3.2

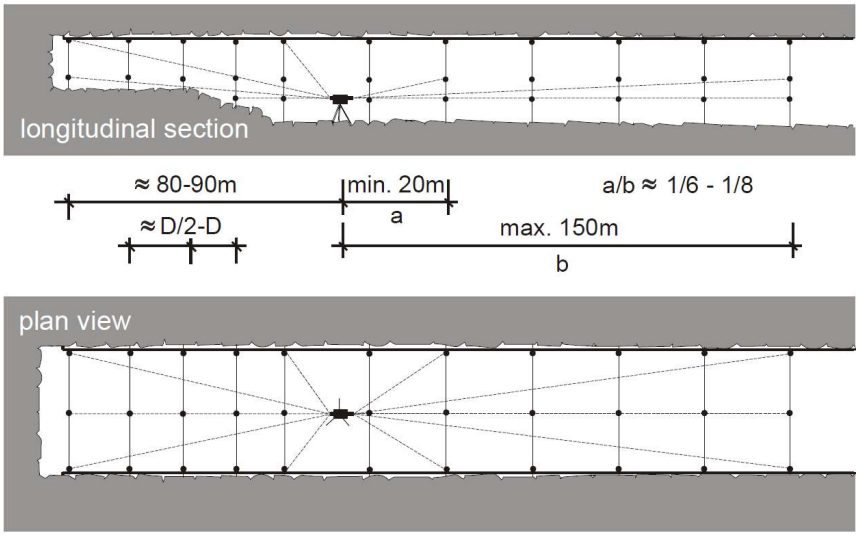

Figure 3.2: Geodetic measurements using the free station method (schematic sketch) *(4)*

A monitoring section (MS) consists of 5 prism targets and is installed every 10 m. One target at each sidewall, one at each shoulder and one at the crown. The position of the targets can be seen in Figure 3.3. The displacements in this plot, and for all further in this format, are upscaled by a factor of 50.

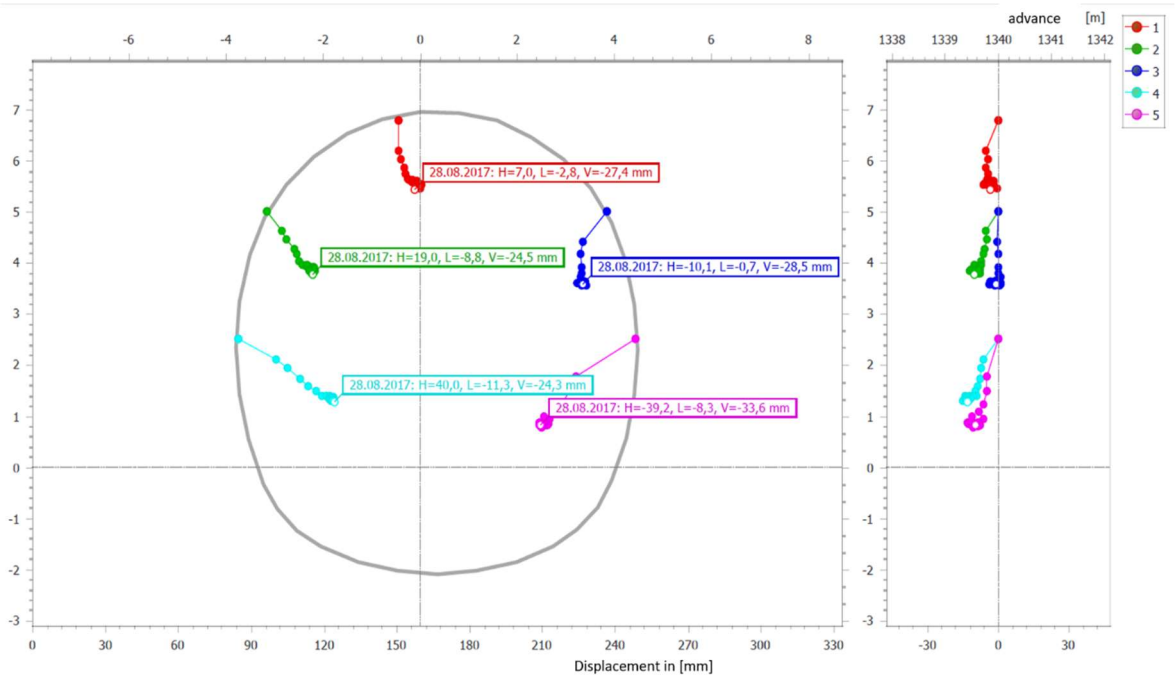

Figure 3.3 Example of a vector plot at chainage 1340 m *(5)*

The measured data was provided in form of displacement-distance-diagrams, displacement-time-diagrams, vector plots and trendlines.

Each direction of movement, horizontal, vertical and longitudinal is plotted separately for the displacement-distance-diagrams as well as for the displacement-time-diagrams. Additionally to the trendlines for every directional movement, also the trendline for the longitudinal rotation of the displacement vector (L/S) was provided.

4 Assessment and Interpretation

In search of comparable attributes to define certain areas of similar system behaviour, it was found, that for chainage 1300m – 1450m the foliation has a rather consistent dip direction towards N-E, only rotating towards S-W at the end of the section, as shown by the stereographic plots in chapter 2.2. Analysing the discontinuity sets, no further conclusive systematics have been encountered.

The longitudinal vector orientation of the right shoulder (target 3 in Figure 4.1) shows a systematic behaviour different from all other measuring points along the circumference. Compared to the normal orientation observed for the longitudinal vector orientation, it is distorted towards the direction of excavation.

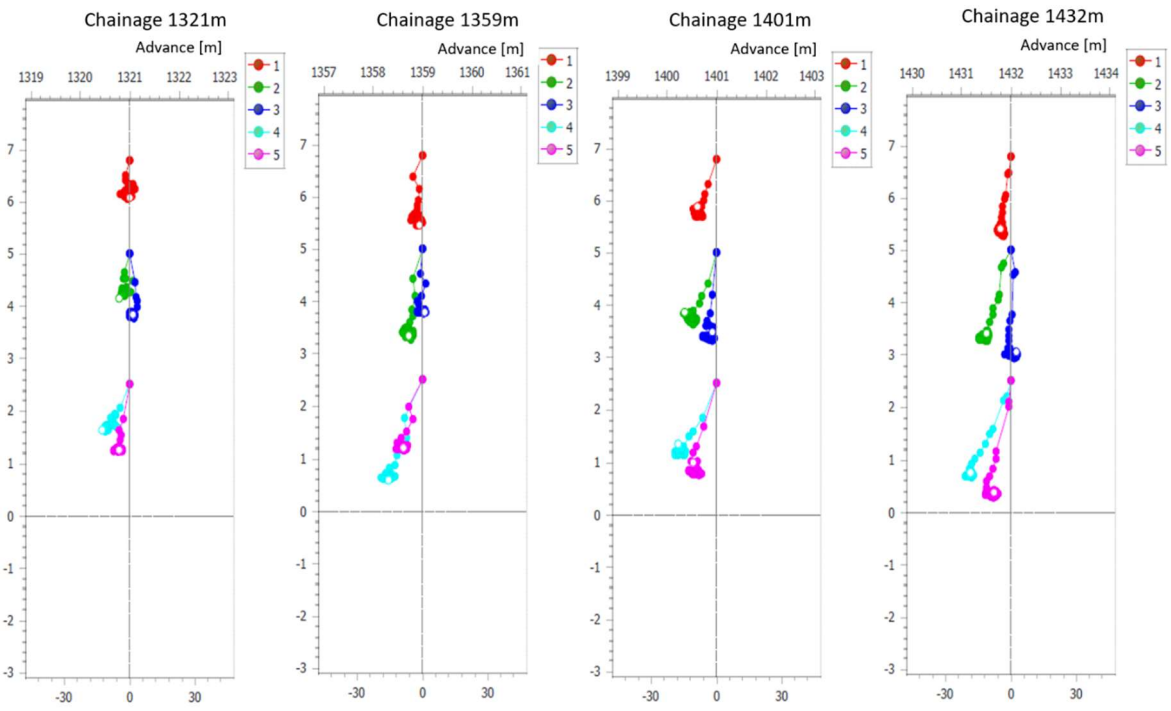

Figure 4.1 Longitudinal vector orientation chainage 1321m - 1432m *(5)*

Regarding the occurring foliation orientation this happens in accordance to Davila Mendez on page 83 of his doctoral thesis “Displacement Analysis in Layered Rock Masses” (6). He states that for discontinuities that dip distorted to the tunnel axis against the direction of drive with a dip angle lower than 75°, the displacement vector on the side the discontinuity is dipping towards, turns in direction of drive. He ascribes this behaviour to a shearing aptitude approximately perpendicular to the weakness plane orientation.

The dip angle of 75° he mentions is valid for the boundary conditions of his analysis. In

general, the systems behaviour changes from a bending aptitude at one side to a sliding aptitude at the other side of the cavity, depending on the discontinuity orientation and strength (6).

Here, the foliation is dipping from left to right, against direction of drive. Therefore, the displacement vectors at the right side should turn further in direction of drive than the one at the left side as schematically depicted in Figure 4.2. This is what can be partially observed here until chainage 1450m as depicted in Figure 4.1 (the position of the measuring points in the cross section can be seen in Figure 3.3) as the deformation vector at the right shoulder performs such a rotation while the vector of the right sidewall does not seem to follow the described systematics.

Furthermore, Davila Mendez stated that the magnitude of deformation should also be larger at the same side the vector turns in direction of tunnelling. In this case at the right-hand side. In contrast to the effect on the vector rotation, the difference in displacement magnitude is not systematically evident along the considered tunnel section chainage 1300 m – 1450 m.

This varying behaviour may be explained by the high degree of fragmentation along the whole considered area. As described in the geological assessment, not only the foliation, but additional joints, slickensides and minor fault zones disturb the rock mass throughout the entire area of the “Halterstelle Eichberg Seitenverschiebung”. The behaviour induced by these additional discontinuities superposes with the effects of the anisotropy of the rock.

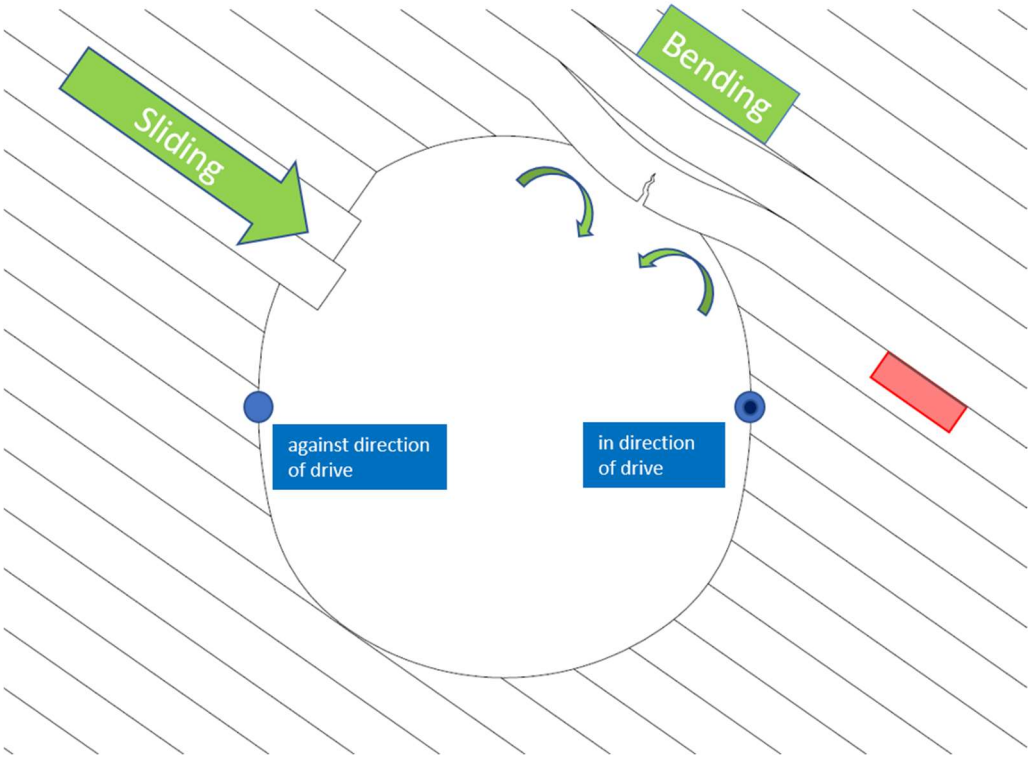

Figure 4.2: Schematically depicted effect of foliation on the longitudinal displacement vector

4.1 Chainage 1340m – 1380m

The systematics described above can only be observed partially at TM 1340. While the right shoulder moves longitudinal in direction of drive, it doesn't noticeable displaces stronger than the left shoulder. The right sidewall is subjected to larger displacements than the left sidewall, but it's behaviour is not compliant with the findings of Davila Mendez as it too should rotate in direction of drive. That the system behaviour is only in partial accordance with Davila Mendez can also here be possibly explained by the high degree of fragmentation of the stratus around the measuring section. The rock mass behaviour is therefore governed by the interaction of multiple discontinuities, and the effect of specific discontinuity sets such as the foliation becomes more difficult to recognize.

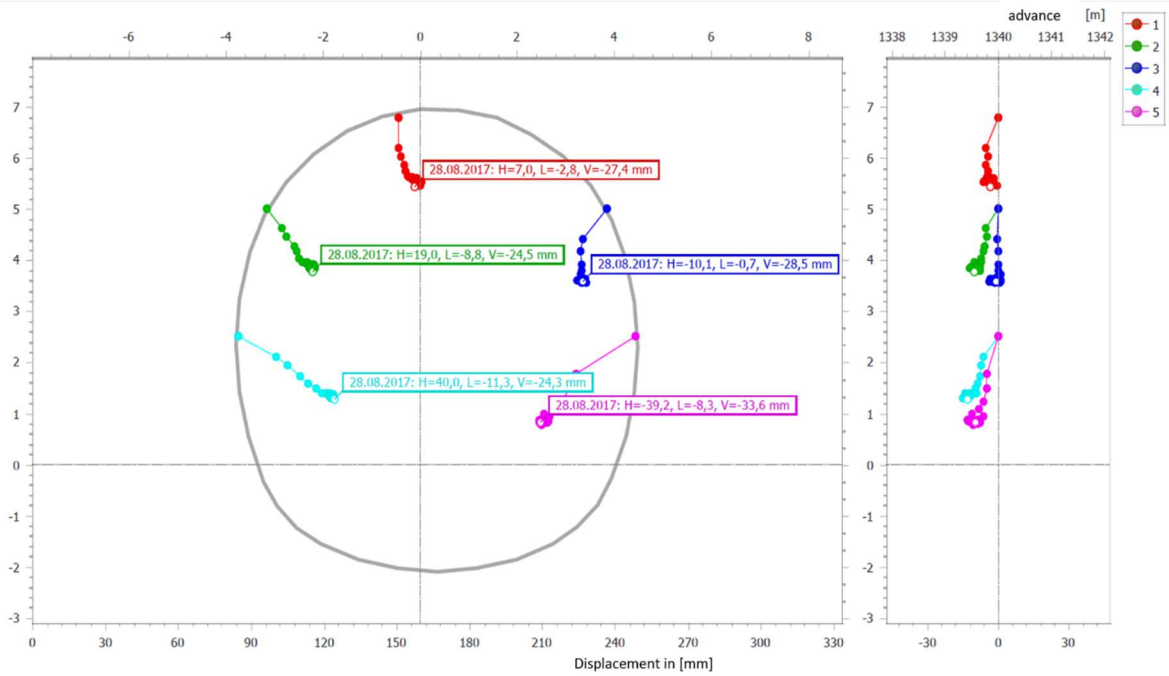

Figure 4.3: Vector plot chainage 1340m *(5)*

In Figure 4.4 the face documentation at chainage 1341.2 m indicates a cataclastic shear band above an area of disintegrated rock. At the crown and at the right sidewall, blocks of schistose quartzite are embedded between the disintegrated and the faulted material. It seems likely that the previously discussed systematics described by Davila Mendez do not entirely adopt for such a varying rock matrix with a high content of disintegrated and cataclastic areas.

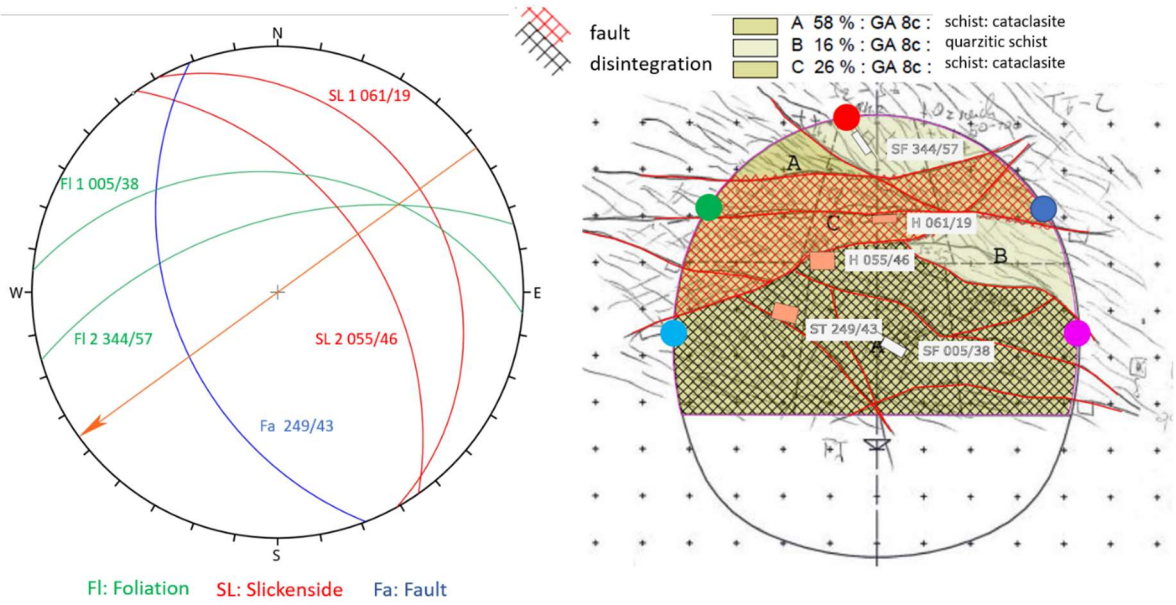

Figure 4.4 Stereographic projection of mapped discontinuities at chainage 1340m (left); Face documentation at chainage 1341.2m (right)

While the same statements regarding the observations at MS 1340m account for the whole range of MS 1300m – 1450m, not every behaviour is entirely explained by them. Additional mechanism become governing and distort the deformation pattern.
Such mechanisms occur between chainage 1340m and 1380m. In this range, deformations occur that do not fully comply with the mapped geological conditions.

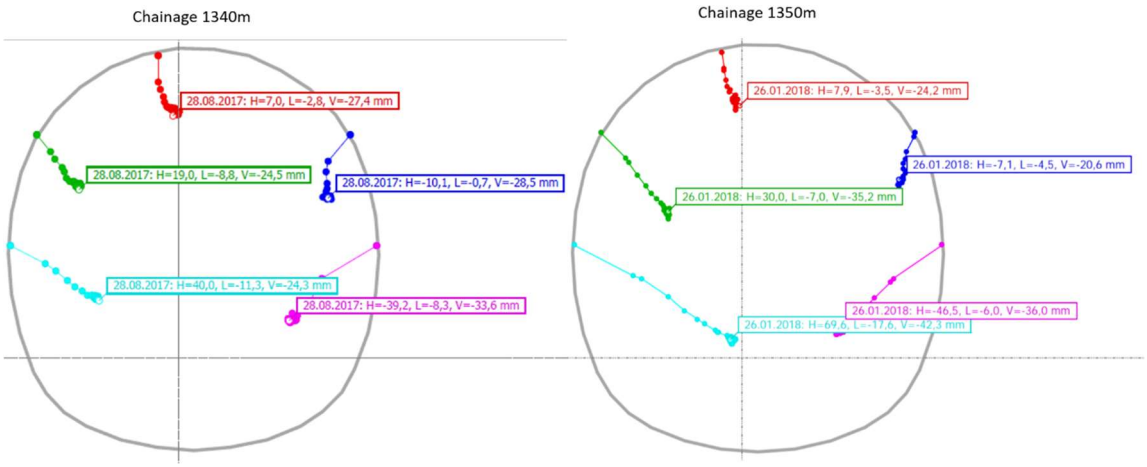

Figure 4.5: Displacement plots of MS 1340m (left) and MS 1350m (right) (5)

In Figure 4.5 it is observable, that the total displacement vector at the left sidewall increases by almost 75% between chainage 1340m and chainage 1350m, the vector at the left shoulder by almost 50% and the vector at the right sidewall increases by 16%.
From MS 1350m to MS 1359m, depicted in Figure 4.6, the deformations decrease at both

the left- and the right-hand side of the tunnel. Still the deformation is asymmetrical, its magnitude is noticeably larger at the left.

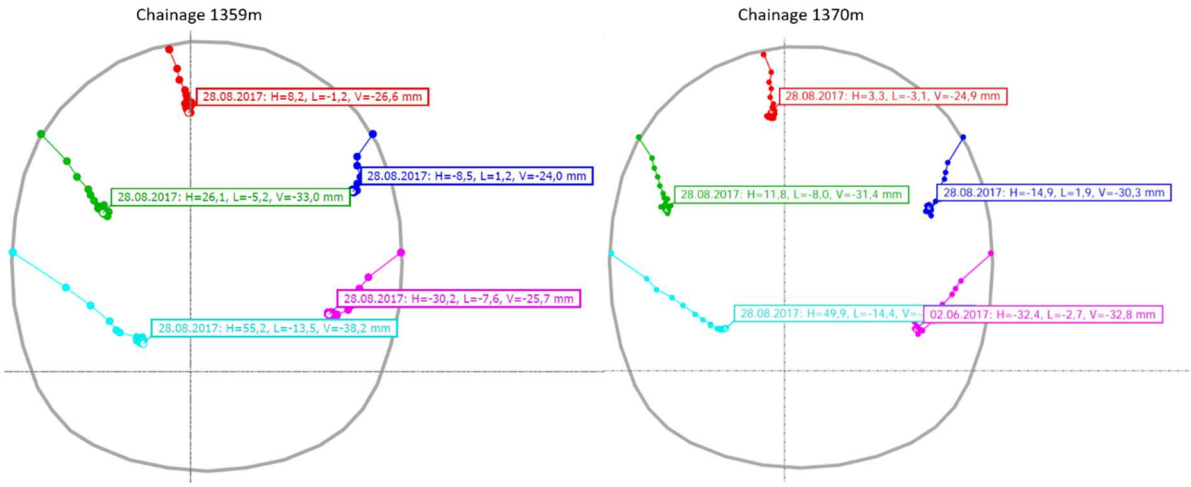

Figure 4.6: Displacement plots of MS 1359m (left) and MS 1370m (right) (5)

Between MS 1359m and 1370m, the displacements further decrease at the left and slightly increase at the right side. This results in a more symmetrical deformation pattern.

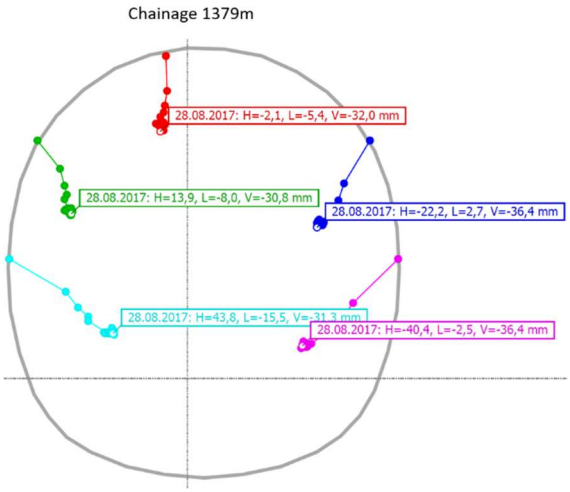

Figure 4.7: Displacement plot of MS 1379m *(5)*

At chainage 1379m (Figure 4.7), the deformation pattern doesn't show a noticeable distorted behaviour anymore.

In Table 4.1 the horizontal (H), longitudinal (L) and vertical (V) final displacement components of each measuring target at each of the mentioned measuring sections are listed and the resulting displacement vector length is calculated using the formula

$$VectorLength = \sqrt{H^2 + L^2 + V^2} \quad . \qquad [4.1]$$

In order to analyse und compare the monitored system behaviour from section to section in a quantitative way, the absolute displacements were calculated for each monitoring target and compared to the displacements at previous sections. The changes between the subsequent sections where normalized to the displacement of the pervious sections. The results are listed in Table 4.1.

	Target	Delta			Vector Length [mm]
		H [mm]	L [mm]	V [mm]	
Chainage 1340 m	Left Sidewall	40	-11.3	-24.3	48.1
	Left Shoulder	19	-8.8	-24.5	32.2
	Crown	7	-0.7	-28.5	29.4
	Right Shoulder	-10.1	-28.1	-66.7	73.1
	Right Sidewall	-39.2	-8.3	-33.6	52.3
				Average	47.0

	Target	Delta			Vector Length [mm]	Δ from previous [%]
		H [mm]	L [mm]	V [mm]		
Chainage 1350 m	Left Sidewall	70.4	-16.6	-42.4	83.8	74
	Left Shoulder	30.4	-7.4	-36.6	48.2	49
	Crown	5.9	-3	-25.9	26.7	-9
	Right Shoulder	-7.1	-4.5	-20.6	22.2	-70
	Right Sidewall	-46.6	-4.8	-38.5	60.6	16
				Average	48.3	3

	Target	Delta			Vector Length [mm]	Δ from previous [%]
		H [mm]	L [mm]	V [mm]		
Chainage 1360 m	Left Sidewall	55.2	-13.5	-38.2	68.5	-18
	Left Shoulder	26.1	-5.2	-33	42.4	-12
	Crown	8.2	-1.2	-26.6	27.9	4
	Right Shoulder	-8.5	1.2	-24	25.5	15
	Right Sidewall	-30.2	-7.6	-25.7	40.4	-33
				Average	40.9	-15

	Target	Delta			Vector Length [mm]	Δ from previous [%]
		H [mm]	L [mm]	V [mm]		
Chainage 1370 m	Left Sidewall	49.9	-14.4	-32	61.0	-11
	Left Shoulder	11.8	-8	-31.4	34.5	-19
	Crown	3.3	-3.1	-24.9	25.3	-9
	Right Shoulder	-14.9	1.9	-30.3	33.8	33
	Right Sidewall	-32.4	-2.7	-32.8	46.2	14
				Average	40.2	-2

	Target	Delta			Vector Length [mm]	Δ from previous [%]
		H [mm]	L [mm]	V [mm]		
Chainage 1380 m	Left Sidewall	43.8	-15.5	-31.3	56.0	-8
	Left Shoulder	13.9	-8	-30.8	34.7	1
	Crown	-2.1	-5.4	-32	32.5	28
	Right Shoulder	-22.2	2.7	-36.4	42.7	26
	Right Sidewall	-40.4	-2.5	-36.4	54.4	18
				Average	44.1	10

Table 4.1: Final displacements at measuring sections from chainage 1340m - 1379m

Analysing the geological situation illustrated in Figure 4.8, the deformations at chainage 1350m are larger and more asymmetrical than the deformations at chainage 1360m. A more expected system behaviour for this situation are greater deformations at the north-east (left in direction of drive) side of the cavity at chainage 1360m since the fault zone is closer to the tunnel there than at chainage 1350m. The increased deformations caused by a discontinuity in vicinity to the cavity are the result of a stress concentration between the tunnel opening and the discontinuity. After excavation, the formed rock pillar between the discontinuity and the cavity attracts more stress since it has a relatively high stiffness compared to its surrounding fault zone. More stress is therefore concentrated close to the tunnel compared to an undisturbed situation. A higher stress state further leads to higher strains.

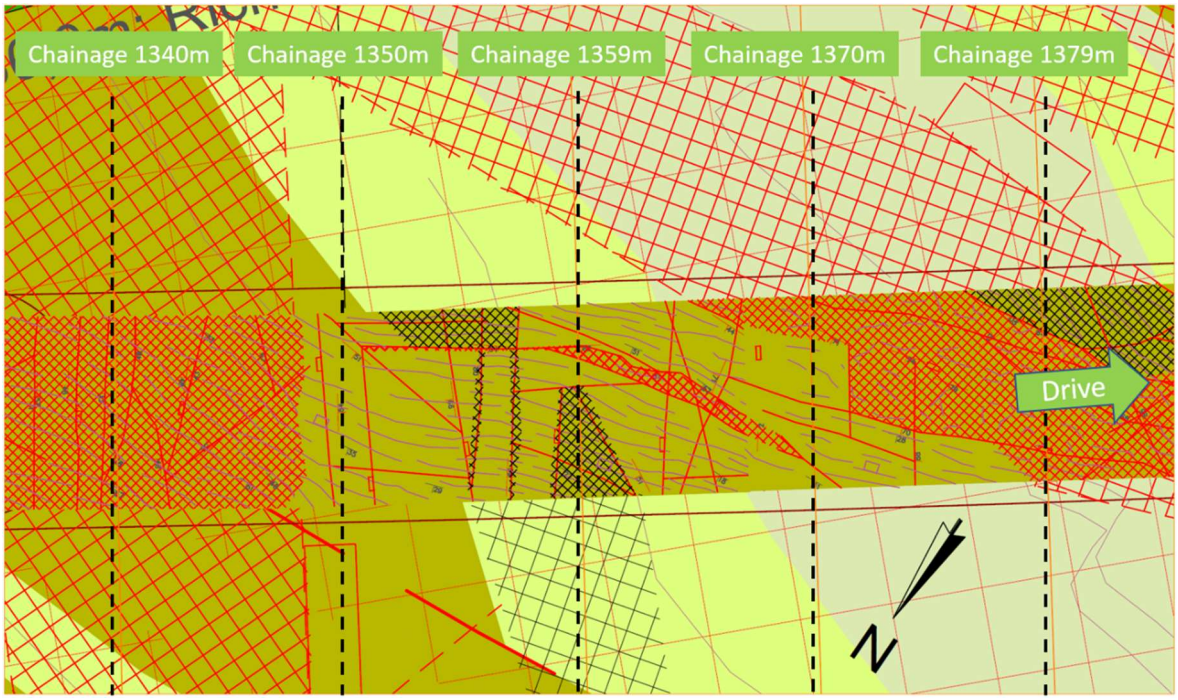

Figure 4.8 Subhorizontal section of MS 1340m to MS 1380m (2)

To check the stated hypothesis for the present case, a 3D analysis using the software RS³ (7) has been performed. A cubic model space was assumed with 150m side length. For the tunnel shape, the proposed geometry for “Regelprofil ZV1” (1) with a height of 9m and a width of 8m has been implemented. The geometry for the model is shown in Figure 4.9.

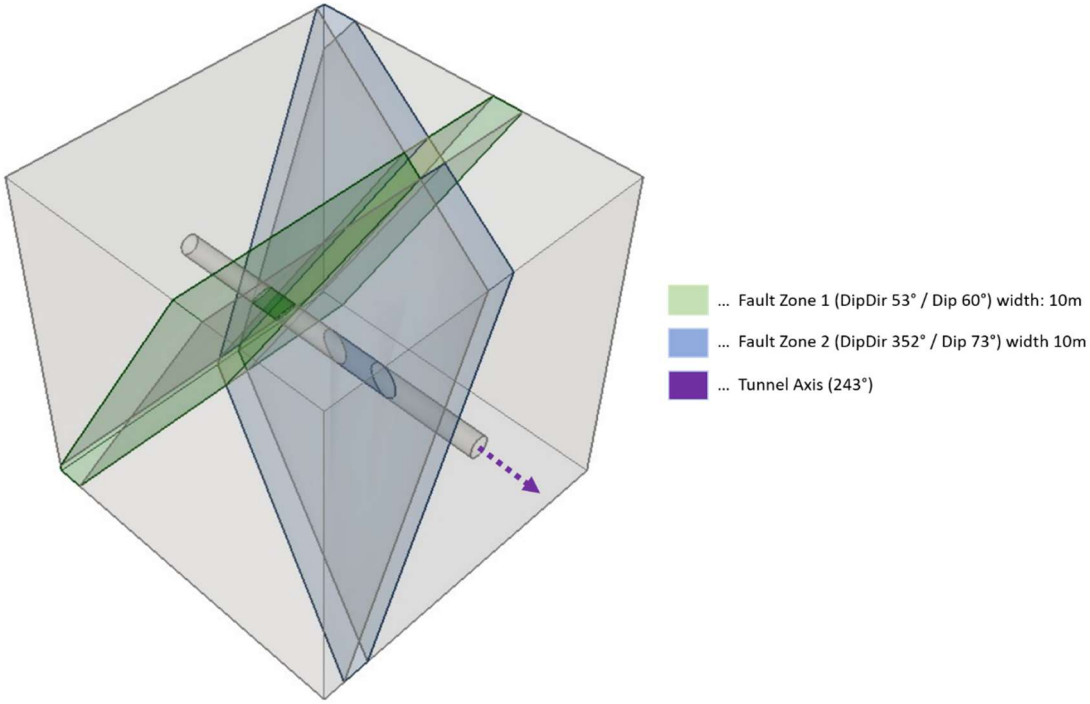

Figure 4.9: RS³ *(7)* model with two fault zones

The objective was to qualitatively show the expected system behaviour occurring between chainage 1340m and 1780m. The model has been based on the geological conditions shown in Figure 4.8. A thickness of 10m was applied to both fault zones.

Rock mass parameters have been chosen according to RMT 2b-2 for the competent rock mass and according to RMT 8c for the fault zones. The parameters can be found in chapter 2.1. The model has been established as a “wished in place” model, meaning that the excavation was modelled in one step, ignoring the sequential construction of the tunnel. Furthermore, no lining, nor the anisotropy of the rock has not been taken into account to simplify the model and the interpretation of the results.

In the contour plots of Figure 4.10, one can observe higher displacements in the area of the left sidewall at chainage 1359m. These results substantiate the previously stated hypothesis that fault zone 2 provokes asymmetry in the deformation pattern at chainage 1359m.

However, the monitored system behaviour contradicts the qualitative system behaviour shown by the numerical analysis of the geological situation, since the measurements indicate a higher deformation at the left sidewall for chainage 1350m than for chainage 1360m. The numerical results on the other hand show higher deformations at chainage 1360m than at chainage 1370m. This leads to the conclusion that either the governing mechanism is a different one than assumed, or the model assumptions do not match the actual situation sufficiently. In the following subsections, potential mechanisms explaining the observed displacement behaviour are analysed.

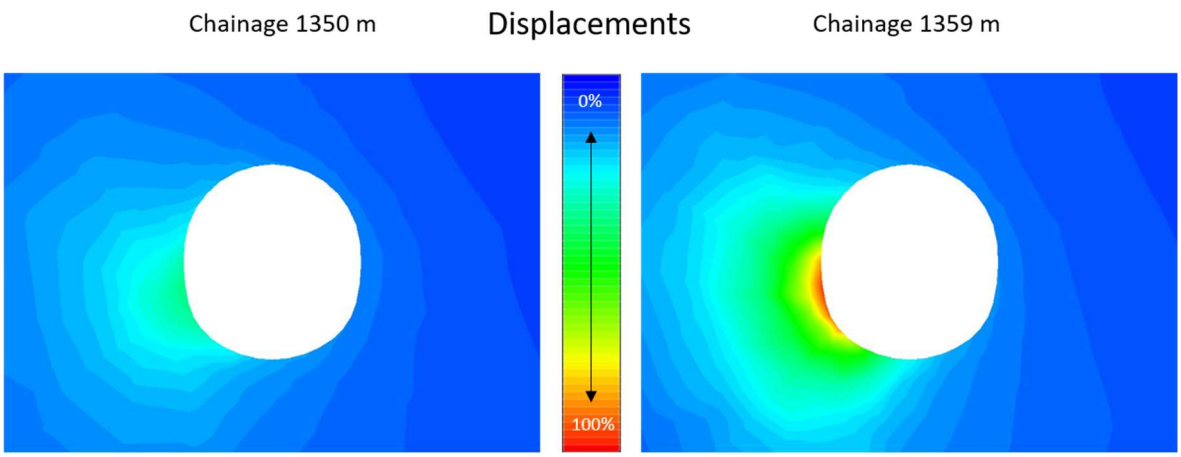

Figure 4.10: Numerical results for the displacements of chainage 1350m and 1359m

4.1.1 Geological Feature

A possible explanation for the unexpected behaviour occurring between chainage 1340m and chainage 1379m could be a mechanically significant geological feature that has not been identified and that lies close to the tunnel cavity. It should be stated here that not every round is mapped geologically because of 24h excavation works. Therefore, single features may not be identified with respect to the generally heterogeneous rock mass. To figure out the most probable origin and location of such a feature, a closer look has been taken at the face documentation of chainage 1340m and chainage 1360m to see if features mapped there should - due to their spatial orientation - theoretically cross the tunnel face at chainage 1350m or should at least strike close to the tunnel.

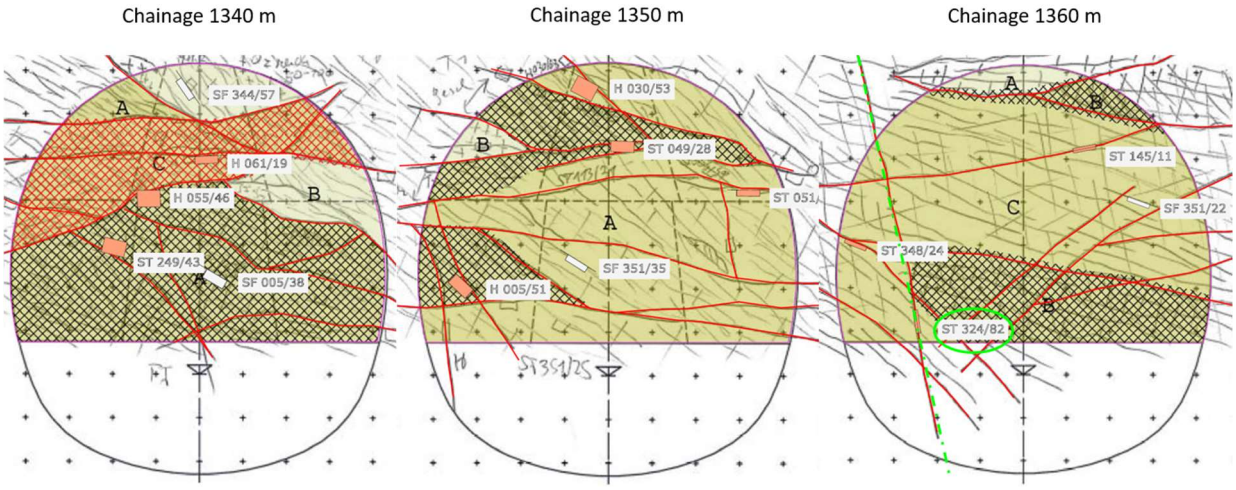

Figure 4.11: Face documentations chainage 1340m, 1350m and 1360m (2)

In the face documentation of chainage 1360m, a very steep fault (marked in green) was

identified on the south-east (left) side of the face, which strikes almost parallel to the tunnel axis. A geometrical construction of the tunnel layout (Figure 4.12) and the spatial orientation of the fault (DipDir 324 / Dip 82) shows that this fault does not leave the cavity until chainage 1350m assuming a continuous orientation of the fault. This geometrical construction underlies the assumption that no unexpected offset, bending folding or rotation of the fault occurs in the observed section. This assumption is encouraged by the constant orientation of the foliation mapped in the face documentations throughout this section. In case the geometric reconstruction matches the actual course of the fault, no influence of the fault is expected.

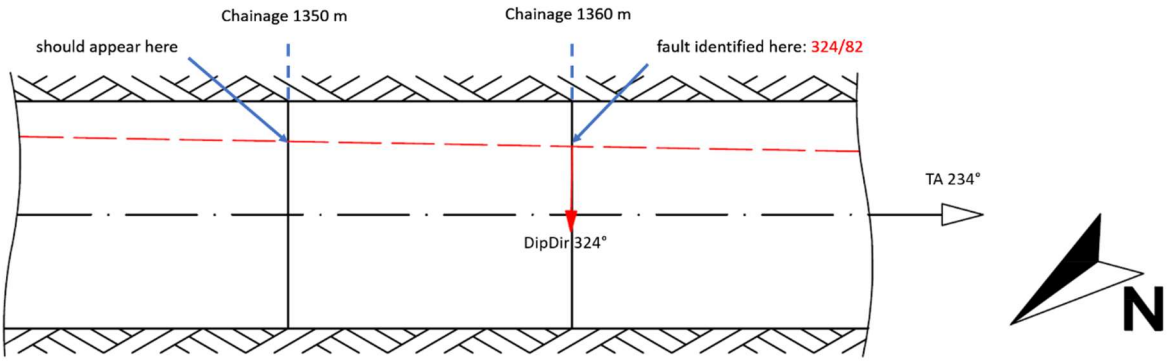

Figure 4.12: Geometrical illustration of the horizontal section chainage 1340m - 1370m

Further, a closer look at the disintegrated zone approaching the tunnel from a NNW to ESE could lead to the assumption that this disintegrated zone continues through the tunnel circumference and extends further in an eastward direction as shown in Figure 4.13, indicated by the yellow hatch.

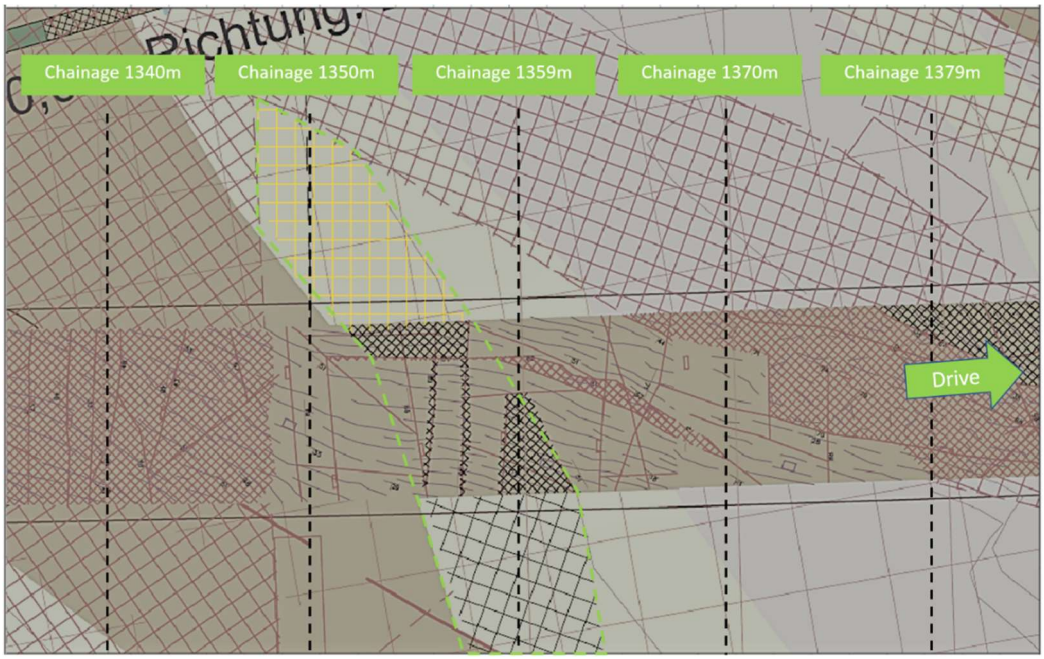

Figure 4.13: Possible continuation of the disintegrated zone

The disintegrated area can also be seen in the face documentation at chainage 1356m, shown in Figure 4.14. There, in the area “D” on the left-hand side, the disintegrated area is part of the disintegrated zone that is assumed to continue eastward. In that face documentation, the rock strength of the area “D” has been documented with 1-5 [MPa], equal to the cataclastic zone encountered at that location. Since the intact rock in this area has already this very low strength, similar to the fault material, and also previous experiences have shown that the rock mass quality of the disintegrated zones does not deviate much from the fault material, it is assumed that the disintegrated zone has similar effects on the system behaviour - in terms of resulting displacements - as the surrounding fault zones.

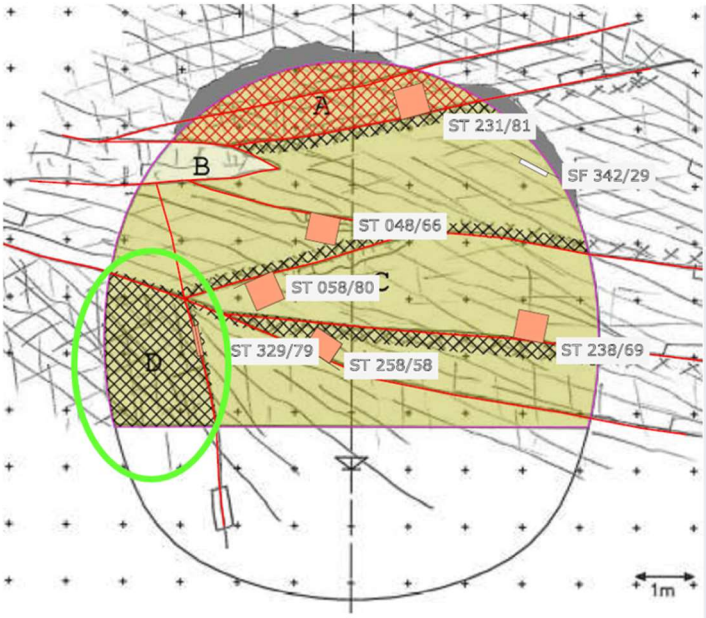

Chainage	Area	Share [%]	Strength [MPa]
1356 m	A	10	1-5
	B	2	19-43
	C	79	5-23
	D	9	1-5

Figure 4.14: Rock strength distribution at chainage 1356m *(2)*

The mechanical potential of the fault zones has been analysed qualitatively with previous FE calculation. Since the disintegrated zone shows similar attributes, a mechanical significance can also be expected. This case has been assumed to be the most probable geological feature that affects the displacement behaviour at chainage 1350m. There is also the possibility that a steep discontinuity passes by in the vicinity of the cavity at this location since such discontinuities occur systematically in this area. However, no hard evidence of such a discontinuity has been identified in the provided geological data. Therefore, a second numerical model has been established to analyse the effect of the disintegrated zone on the system behaviour.

The same parameters have been chosen as for the previous model, RMT 2b-2 for the competent rock mass and RMT 8c for the fault zones and the disintegrated zone.

Again, the model has been established as “wished in place”.

The orientation of the disintegrated zone has been taken from the geological subhorizontal section as depicted in Figure 4.13.

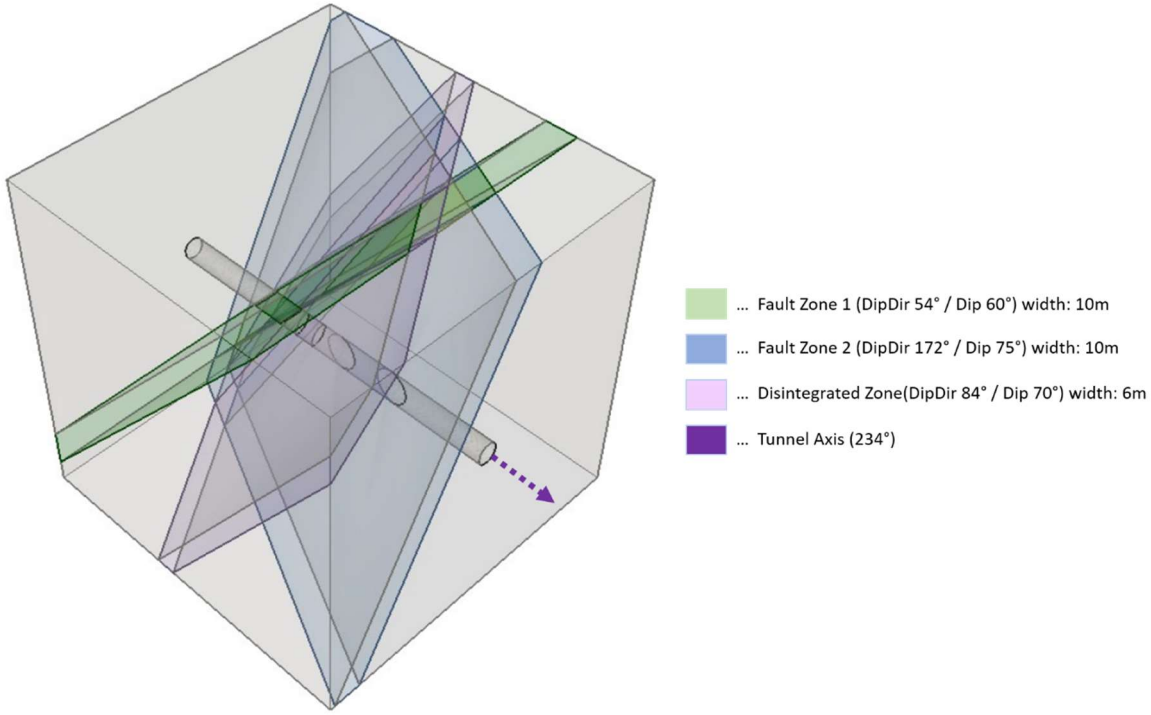

Figure 4.15: 3D FE model with disintegrated zone

The results in Figure 4.15 now show that, as expected, the displacements at chainage 1350m are noticeable larger than the ones at chainage 1360m. The continuation of the disintegrated zone of the left side of the tunnel is plausible, and also the results qualitatively fit the monitored system behaviour (compare with Figure 4.5: higher deformations at the left side of the tunnel than at the right side).

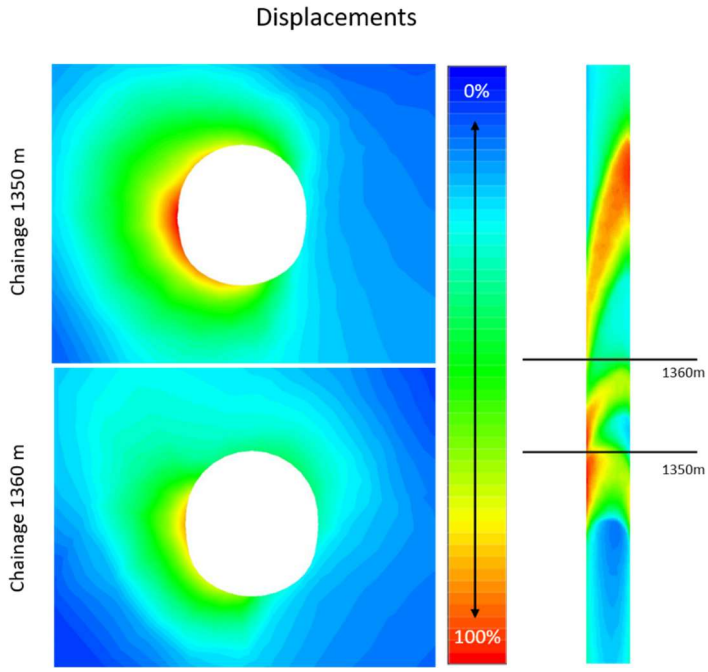

Figure 4.16: Total Displacements with Disintegrated Zone

4.1.2 Sliding along discontinuities

Further, it has been investigated if the deformation vectors indicate a possible sliding failure along or opening of the encountered discontinuities. Of special interest is, if the displacement of the left sidewall at chainage 1350m could be explained by such a behaviour. In order to do so, the vector orientation has been calculated from the original position of the according target to its final position. First, the strike of the vector has been calculated relative to the strike direction of the face by using the formula

$$\tan\gamma = \frac{L}{H} \quad . \qquad [4.2]$$

L ... final longitudinal displacements
H ... final horizontal displacements

and has then been transformed into the local coordinate system of the tunnel.

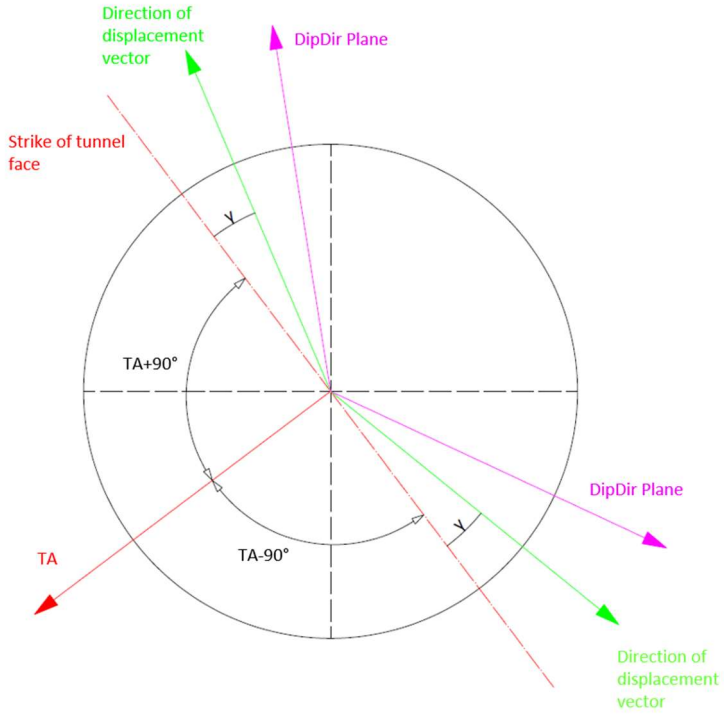

Figure 4.17: Vector Direction

Later, the Dip angle has been calculated using the formula

$$\tan(Dip) = \frac{V}{H} \quad . \qquad [4.3]$$

V ... final vertical displacements
H ... final horizontal displacements

Goricki (8) analysed the influence of discontinuities on the displacement vector behaviour and also established certain values for the deviation of the vectors from a radial direction in relation to the discontinuity orientation. Of interest for this analysis though was to search for displacements that have been provoked by a sliding failure, especially it is aimed to determine whether the large deformations occurring at chainage 1350m can be related to such a behaviour. For such cases, the mayor component of the displacement vector should follow the orientation of the discontinuity to a major proportion.

The criterion to determine whether a sliding occurred along an encountered discontinuity was that the dip direction of the vector should not be deviating more than $\pm$ 10° from the dip direction of the discontinuity while also the dip angle of the vector and the discontinuity should not deviate more than $\pm$ 10°. The criterion to determine whether an opening of the discontinuity occurs was formulated as $DipDir_{Vector} + 180° - DipDir_{plane} < 10°$

This procedure may not be accurate in all cases. Especially, for displacement vectors for which the sliding takes up only a minor proportion of the total displacement, but for vectors that are predominately influenced by a sliding aptitude, and such are of interest for this analysis, a compliance between the discontinuity orientation and the displacement vector direction should be evident within the defined range of $\pm$ 10°.

As shown in Table 4.2, none of the indicated possible sliding or opening failures along a discontinuity qualifies as explanation.

4.1.1 Conclusion

After performing the above described analyses, it seems that the most probable cause for the large deformations at chainage 1350 m - compared to the deformations behind and ahead of this chainage - is the disintegrated zone mapped at chainage 1351.2 m, which is likely to continue in ESE direction.

Displacement Vectors				Discontinuities				Sliding						Opening					
	Target	Orientation			Type$_i$	Orientation			Fl1	Fl2	Sl1	Sl2	Fa1		Fl1	Fl2	Sl1	Sl2	Fa1
		DipDir [°]	Dip [°]			DipDir [°]	Dip [°]												
Chainage 1340	Left Sidewall	339	31		Fl 1	344	57	Left Sidewall							Left Sidewall				
	Left Shoulder	348	52		Fl 2	5	38	Left Shoulder		x					Left Shoulder				
	Crown	329	76		Sl1	52	71	Crown							Crown				
	Right Shoulder	73	81		Sl 2	55	80	Right Shoulder							Right Shoulder				x
	Right Sidewall	131	41		Fz 1	249	43	Right Sidewall							Right Sidewall				
									Fl1	Sl1	Sl2	Fa1	Fa2		Fl1	Sl1	Sl2	Fa1	Fa2
Chainage 1350	Left Sidewall	336	31		Fl 1	351	35	Left Sidewall							Left Sidewall				
	Left Shoulder	337	50		Sl 1	5	51	Left Shoulder							Left Shoulder				
	Crown	350	77		Sl 2	30	53	Crown							Crown				
	Right Shoulder	149	4		Fz 1	49	28	Right Shoulder							Right Shoulder				
	Right Sidewall	137	40		Fz 2	51	15	Right Sidewall							Right Sidewall				
									Fl1	Fa1	Fa2	Fa3			Fl1	Fa1	Fa2	Fa3	
Chainage 1360	Left Sidewall	337	35		Fl 1	351	22	Left Sidewall			~				Left Sidewall				
	Left Shoulder	334	52		Fz 1	324	82	Left Shoulder							Left Shoulder				
	Crown	331	73		Fz 2	348	24	Crown							Crown				
	Right Shoulder	151	70		Fz 3	245	11	Right Shoulder							Right Shoulder		~		
	Right Sidewall	129	40					Right Sidewall							Right Sidewall				
									Fl1	Fz1					Fl1	Fa1			
Chainage 1370	Left Sidewall	339	33		Fl 1	355	41	Left Sidewall							Left Sidewall				
	Left Shoulder	357	69		Fz 1	352	71	Left Shoulder		x					Left Shoulder				
	Crown	319	27					Crown							Crown				
	Right Shoulder	150	64					Right Shoulder							Right Shoulder				
	Right Sidewall	138	45					Right Sidewall							Right Sidewall				
									Fl1	Sl1	Fa1	Fa2			Fl1	Sl1	Fa1	Fa2	
Chainage 1380	Left Sidewall	342	36		Fl 1	344	71	Left Sidewall							Left Sidewall				
	Left Shoulder	353	66		Sl 1	112	51	Left Shoulder			x				Left Shoulder				
	Crown	74	86		Fz 1	351	64	Crown							Crown				
	Right Shoulder	150	59		Fz 2	344	71	Right Shoulder							Right Shoulder				
	Right Sidewall	139	42					Right Sidewall							Right Sidewall				

Fl ... Foliation
Sl ... Slickenside
Fa ... Fault Zone
x ... match
~ ... maybe

Table 4.2: Sliding / Opening Mechanism

4.2 Kink in Displacement Vector

A further phenomenon that can be observed throughout the whole area of the “Haltestelle Eichberg” fault system, is a kink in the displacement vector. This kink occurs preferably at the left and the right shoulder of the tunnel profile. Some examples are depicted in Figure 4.18, highlighted by the blue ellipsis. It appears that - at first - the tunnel liner deforms in almost radial direction, as it would be the case for a homogeneous rock mass and an isotropic stress state. At a certain point the displacement path changes to an almost vertical direction. The systematic occurrence indicates that this phenomenon is not caused by measurement inaccuracy.

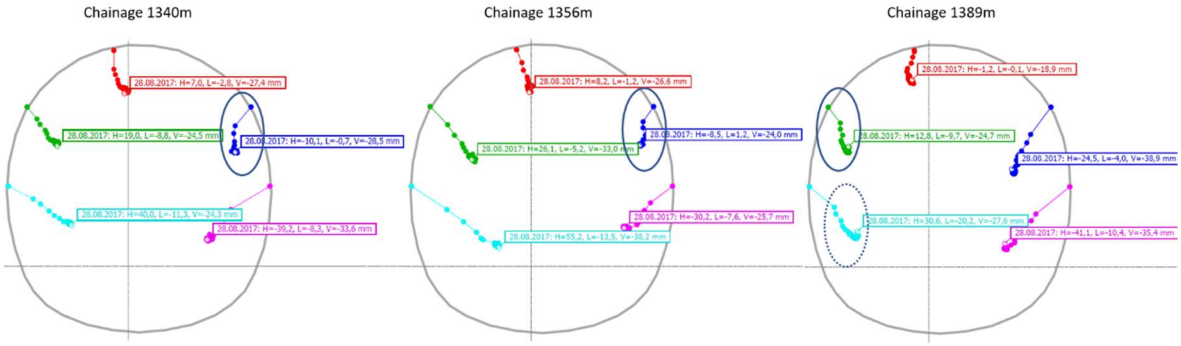

Figure 4.18: Displacement vectors containing a kink *(5)*

The radial deformation preceding the vertical deformation indicates that a change of stress state is necessary to mobilise the vertical deformations. For further investigation of this mechanism, a 2D numerical model has been established in the FE application RS² (9). In the model, only the top heading has been excavated. The anisotropy of the rock was taken into account using the ubiquitous joint feature of the RS² numerical code. The shotcrete support has been applied with the liner feature and an interface has been defined to simulate a weak bond between the liner and the surrounding rock mass in order to enable relative movement between the rock mass and the liner. To simulate the overburden at the area of interest, a constant field stress of 3.78 MPa has been applied. This value corresponds to an overburden of 140m by a specific weight of 2.7 t/m³.

Since it has been assumed that the change of stress state in the vicinity of the cavity leads to the observed phenomena, it is of great interest for the numerical 2D analysis to simulate the 3D effects of an advancing tunnel face on the secondary stresses around the tunnel. Those 3D effects can be considered using the longitudinal displacement profile (i.e. development of radial displacements with increasing distance of the face of a circular tunnel in an isotropic, homogeneous rock mass) as exemplary depicted in Figure 4.19 where a best-fit curve (10) for the measurement data taken by Chern (11) is depicted.

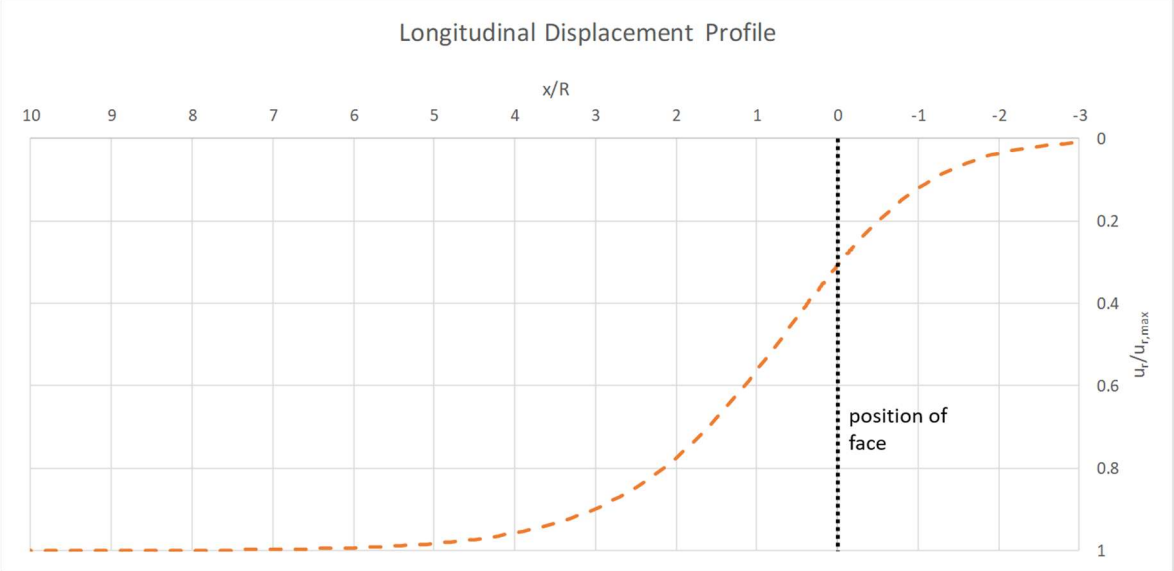

Figure 4.19: Best-fit curve of an LDP encountered at the Mingtam Power Cavern Project

In his Master´s Thesis, Pilgerstorfer (12) introduces a method that incorporates a relationship between the development of the radial displacements in longitudinal direction and an equivalent support pressure at the corresponding distance x from the face. Hence, an internal pressure that yields equivalent displacements in combination with the acting rock pressure. He back calculated the necessary support pressure for the confined state from the closed form solution of Feder and Arwanitakis (13) to which he also scaled the results of his numerical simulations to facilitate further mathematical processing. Eventually, he established the equation

$$\lambda_{(x)} = \lambda_{face} * \xi^{1.2} * \left(\frac{l_{\inf\, l} - x}{l_{\inf\, l} * \xi + x} \right)^{1.2} \qquad [4.4]$$

$\lambda_{(x)}$ … equivalent support pressure coefficient at observed point x

λ_{face} … equivalent support pressure coefficient at the face (pre-relaxation factor)

ξ … fitting parameter

$l_{\inf\, l}$ … influenced length behind face

x … distance to face

He established the equation in a way that it is independent of geometric parameters as they are dealt with by assuming a circular tunnel and the establishing of an unitless variable η describing the ration between the plastic radius and the tunnel radius. The friction angle is further influencing the equation as it is used to span the interpolation surface in the coordinate system for the calculation of λ_{face} and ξ respectively. For further information

about the finding of the equation [4.4, its application and the explanation of its parameters, the reader is kindly forwarded to the work of Pilgerstorfer.

It was decided that utilizing the method of Pilgerstorfer, a satisfying simulation of the 3D effect on the longitudinal displacement profile can be achieved in a 2D numerical simulation. The rock mass parameters, as shown in Table 4.3, have been chosen on the basis of RMT 2b-2.

Table 4.3: Rock Mass Properties

Parameter	Unit	Value
c	[MPa]	1.5
φ	[°]	24
E	[GPa]	1.5

For an appropriate simulation of the continuous advance of the face, a total of 8 values, listed in Table 4.4, have been generated for $\lambda_{(x)}$. Since the usual performed round length in that RMT is 1m, $\lambda_{(x)}$ has been calculated once at one round length distance from the face.

.

Table 4.4: Observed points and equivalent support pressure coefficients

Distance to Face	1m	2m	3m	5m	10m	15m	20m	Inf.
$\lambda_{(x)}$	0.4	0.26	0.18	0.1	0.05	0.02	0.01	0

Applying Pilgerstorfers method to the herein discussed case, λ_{face} is found at a value of 0.77. The yielded values for $\lambda_{(x)}$ represent a proportion of the primary stress state. The values for $\lambda_{(x)}$ multiplied with the value of the primary stress - 3.78 MPa - have then been applied to the RS² model as an internal pressure on the cavity as shown in Figure 4.20. For each value, a separate phase has been generated in the model, so a differentiated analysis of the influence of the advancing face on the displacements was feasible.

The calculation was separated in 10 phases. The first phase represents the initial situation prior to excavation (Figure 4.20 a). In the second phase (Figure 4.20 b), the excavation is conducted and an internal pressure of $p_i = \lambda_{(1m)} \cdot p_{field}$ is applied as schematically depicted in Figure 4.20.

The application of the internal pressure has been conducted constantly around the entire perimeter. In Phase 3, the shotcrete liner is applied to the system, while the internal pressure is active and still representing a distance of 1m to the face. In the following phases, the internal pressure is reduced stepwise according the values listed in Table 4.4. Phase

10 (Figure 4.20 c) represents the final situation after no further influence of the face is acting on the observed section.

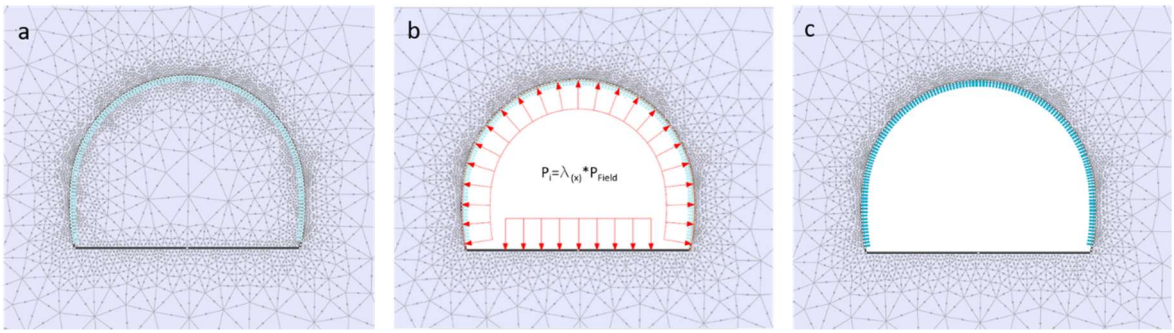

Figure 4.20: Modelling sequence

The liner has been modelled linear elastic featuring the properties in Table 4.5.

Table 4.5: Liner Properties

Parameter	Unit	Value
width	[cm]	25
E	[GPa]	1.5

For the matter of finding correlations between the kink behaviour of the displacement vectors in the sectional plot and geologic features, the chainage of every cross section containing a kink in the displacement vector has been noted, together with the geological peculiarities at the according chainage. Also, the subsequent cross sections containing no kink were analysed.

For cross sections where no geological peculiarity could be found, the angle between the dip direction of the foliation and the direction of the tunnel axis has been averaged once for cases where the vector at the right side shows a kink, and once for cases where the vector on the left side.

For the angle between the foliation and the tunnel axis, a case separation has been introduced where a positive value corresponds to a foliation dipping from left to right and a negative value for a foliation that dips from right to left relatively to the tunnel axis. Further, a value lower than 90° represents dipping against direction of drive, while a value higher than 90° represents a dipping in direction of drive.

Looking at the results in Table 4.6, it can be stated that the foliation orientation shows correlative behaviour with the mechanism underlying the kink in the displacement vector in cases where no further geological peculiarity could be found.

The mean value of the angle between the dip direction of the foliation and the tunnel axis is -48° for cases where the vector kinks at the right side while the mean value for cases where

the vector kinks at the left side is 7°.

For the establishing of these values, only cross sections that are not likely to be influenced by geological features other than the foliation have been included in this calculation. Those geological features mostly refer to vertical faults close to the cavity.

If the cross sections containing such geological features are included in the calculation, no significant difference in the mean foliation orientation can be observed between the case of a displacement vector kinking at the left shoulder and the case of the displacement vector kinking at the right shoulder. Therefore, it seems very probable that those vertical faults close to the cavity also have a significant influence on the formation of a kink in the displacement vector.

To find out whether the hypothetical correlation between the foliation orientation, the vertical faults and the displacement vector can be substantiated, several numerical calculations have been conducted. While the general modelling sequence was kept as previously described, the model has been established in several variations to identify the governing elements of the system behaviour.

Table 4.6: Cross-sections containing kink performing displacement vectors

Chainage [m]	Foliation		Tunnel Axis [°]	Angle to TA [°]	Kink	Side	Significant geological feature
	DipDir [°]	Dip [°]					
1312	13	42	234	-41	no		
1321	18	51	234	-36	no		
1331	354	52	234	-60	yes	right	
1340	344	57	234	-70	yes	right	
1350	351	35	234	-63	-		
1359	351	22	233	-62	yes	right	
1370	355	41	233	-58	no		
1379	344	71	233	-69	yes	left	vertical fault at left shoulder
1389	320	21	233	-93	yes	left	vertical fault at left and right shoulder
1401	35	58	233	-18	no		
1412	375	27	232	-37	yes	right	vertical fault right
1422	7	35	232	-45	yes	right	
1432	32	53	232	-20	no		vertical fault right
1439	75	55	232	23	no		
1459	74	21	232	22	yes	left	
1470	126	28	231	75	no		
1482	101	21	231	50	yes	left	
1491	42	43	231	-9	yes	left	vertical faults at left shoulder
1498	327	5	231	-84	no		
1511	11	32	231	-40	yes	left	
1522	17	33	230	-33	yes	both?	highly fractured; horizontal fault
1530	322	16	230	-88	yes	left	highly fractured; leftward dipping slickensides
1539	338	20	230	-72	yes	right	
1551	321	59	229	-88	yes	right	
1563	60	20	229	11	no		
1573	73	41	229	24	no		
1581	47	52	229	-2	no		
1592	71	38	229	22	yes	left	
1603	54	47	228	6	yes	right	multiple faults right
1615	141	11	228	93	no		

mean angle from TA when left	average dip when kink
7	36
mean angle from TA when right	
-48	

4.2.1 Foliation as dominant anisotropy in Rock Mass

The foliation (depicted in green in Figure 4.21) was modelled using the ubiquitous joint option in RS². Four different apparent angles have been analysed: 15°, 30° 45° and 50°, dipping from left to right as it mostly occurs in the area between chainage 1340m and chainage 1450m. A Mohr Coulomb slip criterion has been chosen for the ubiquitous joint feature and the strength parameters shown in Table 4.7 were applied.

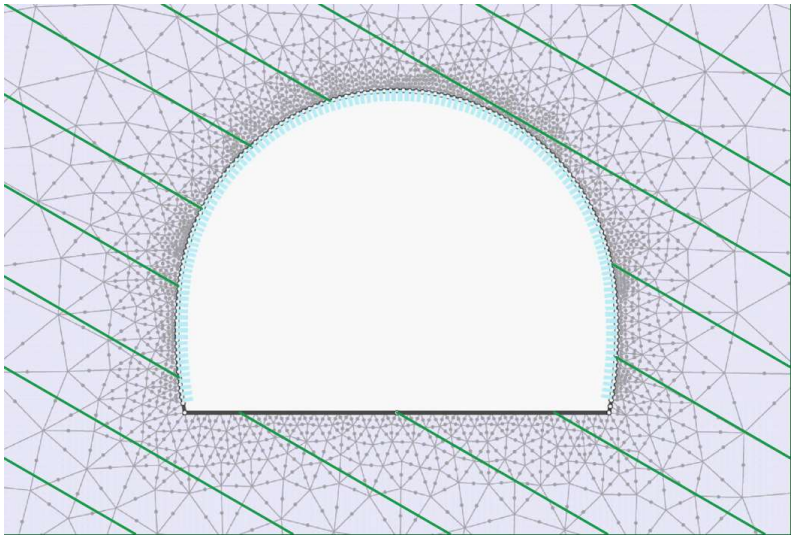

Figure 4.21: Model for dominant foliation

Table 4.7: Parameters Foliation 1. Variant

Parameter	Unit	Value
c	[MPa]	0
φ	[°]	24

Figure 4.22 shows the displacement vectors for the simulated models featuring a mechanically significant foliation, each of them with a different foliation dip angle. Each point represents the displacement value at a separate phase (internal stress reduction). The first point, at the origin, represents the situation before the excavation influences the primary stress state at the observed section. Highlighted in the coloured boxes is the proportion of the displacement, that happens before the zero reading under the assumption, that the first measurement is taken 1m behind the face.

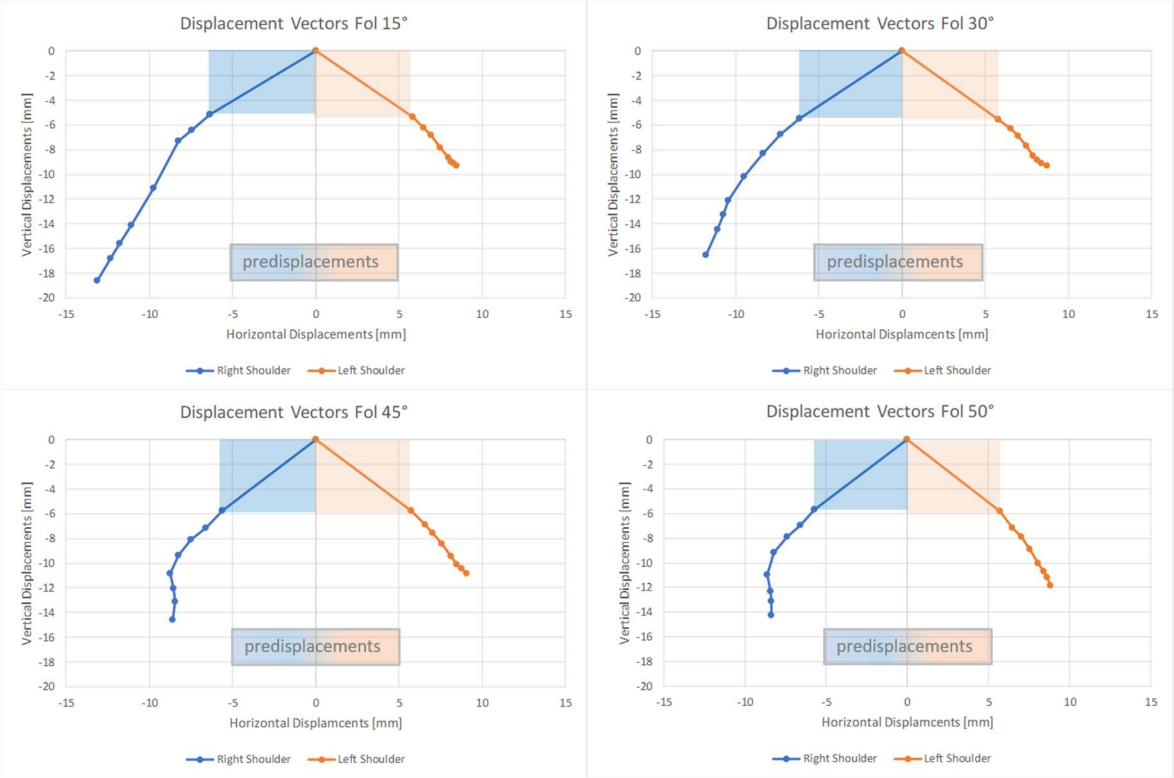

Figure 4.22: Displacement vectors of left and right shoulder (dominant foliation)

In the first two models featuring a foliation with a dip angle of 15° and of 30°, respectively, the displacement vectors do not feature a kink. However, for the models with a dip angle of the foliation of 45° and 50°, a kink of the displacement vector of the right shoulder can be observed, similar to the observations at site.

In Figure 4.23, Figure 4.24 and Figure 4.25, the plastic shear strain is depicted, overlaid by the yielded elements. These figures show the results for the model simulating a dip angle of 45° for the foliation.

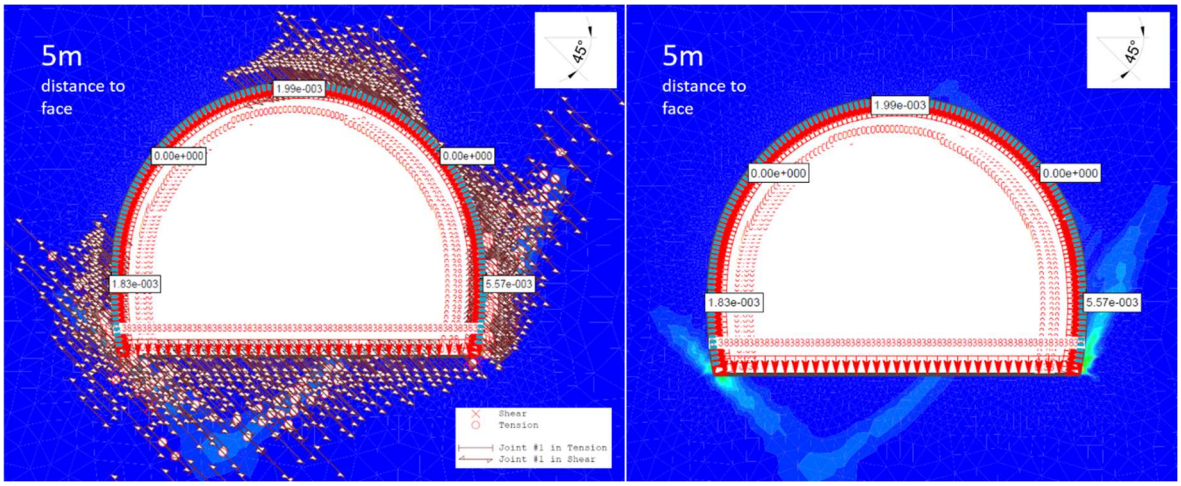

Figure 4.23: 5m distance to face left: yielded elements (left), plastic shear strains (right)

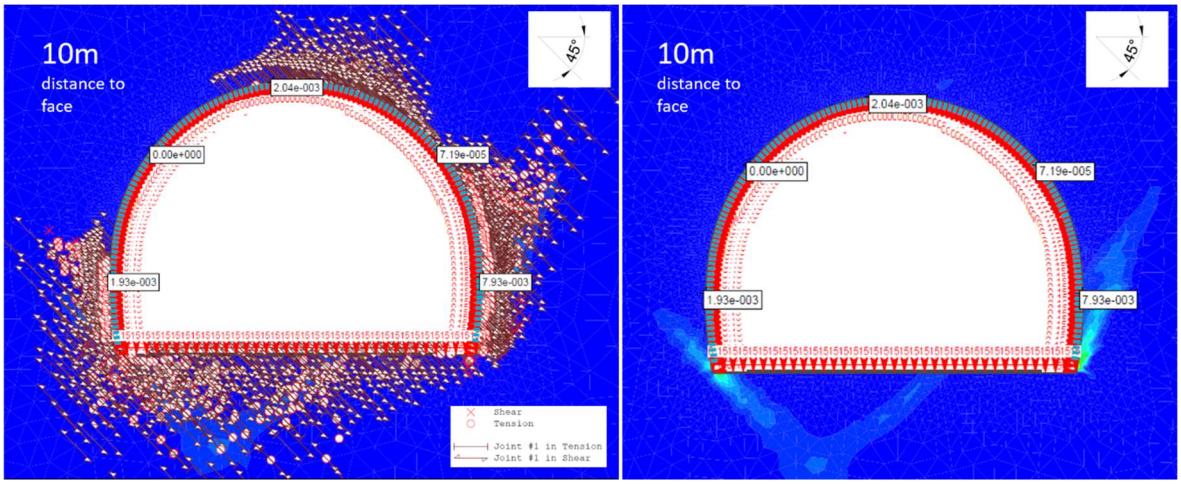

Figure 4.24: 10m distance to face left: yielded elements (left), plastic shear strains (right)

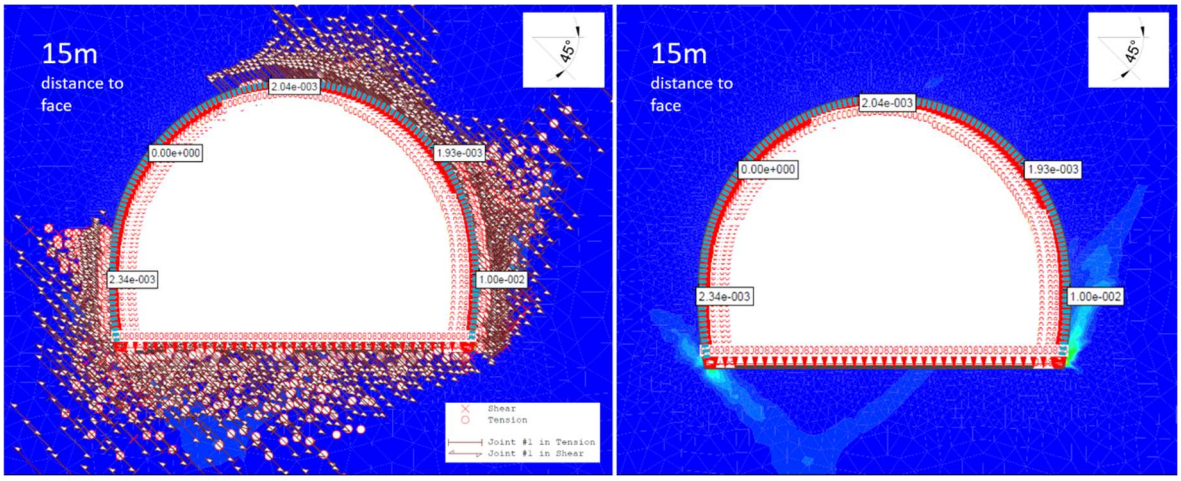

Figure 4.25: 15m distance to face left: yielded elements (left), plastic shear strains (right)

The values in the text boxes at the tunnel boundary represent the magnitude of the plastic shear strain at the according position. It can be seen that in the area of the right shoulder no plastic shear strain was generated when distances smaller than 10m to the face where simulated. At phase 7 (10m distance to face) plastic shear strains occur in the vicinity of the right shoulder. At phase 8 (15m distance to face) severe shearing can be observed around the right shoulder. These observations lead to the conclusion that the generation of the kink in the displacement vector correlates with a mobilisation of the shearing potential of the simulated foliation in the according area.

4.2.2 Vertical joint as dominant anisotropy in rock mass

Very steep faults and slickensides that strike almost parallel to the tunnel axis occur quite systematically over large parts of the “Haltestelle Eichberg” fault system. That for, and because Table 4.6 also indicates a correlation, the influence of those faults on the generation of displacement vectors containing a kink had to be taken into consideration. Various implementations of such a vertical joint have been conducted in the model, but a single discrete joint has proven to deliver the most comprehensible results. No further anisotropy has been modelled as demonstrated in Figure 4.26.

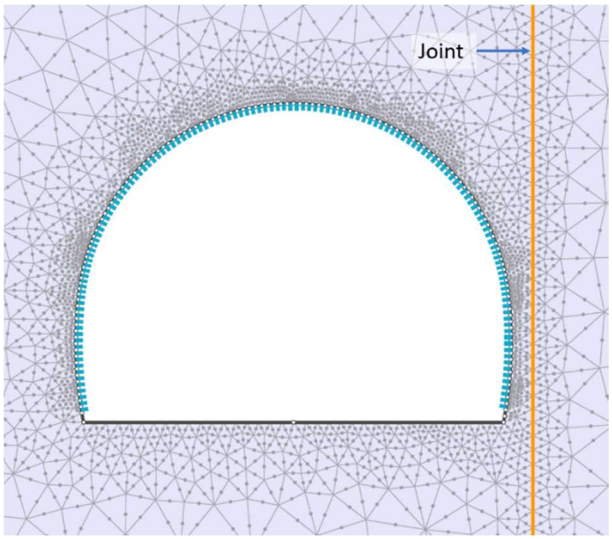

Figure 4.26: Model with discrete vertical joint

The parameters of the joint have been chosen in a way, that it becomes mechanically active. The parameters where applied according to Table 4.8. Since the finding of governing features provoking the mechanism was the general objective of this analysis, rather than the back-calculation of exact values, this proceeding has been found appropriate.

Table 4.8: Parameters Joint

Parameter	Unit	Value
Joint Normal Stiffness	[MPa/m]	10,000
Joint Shear Stiffness	[MPa/m]	1,000
c	[MPa/m]	0
φ	[°]	20

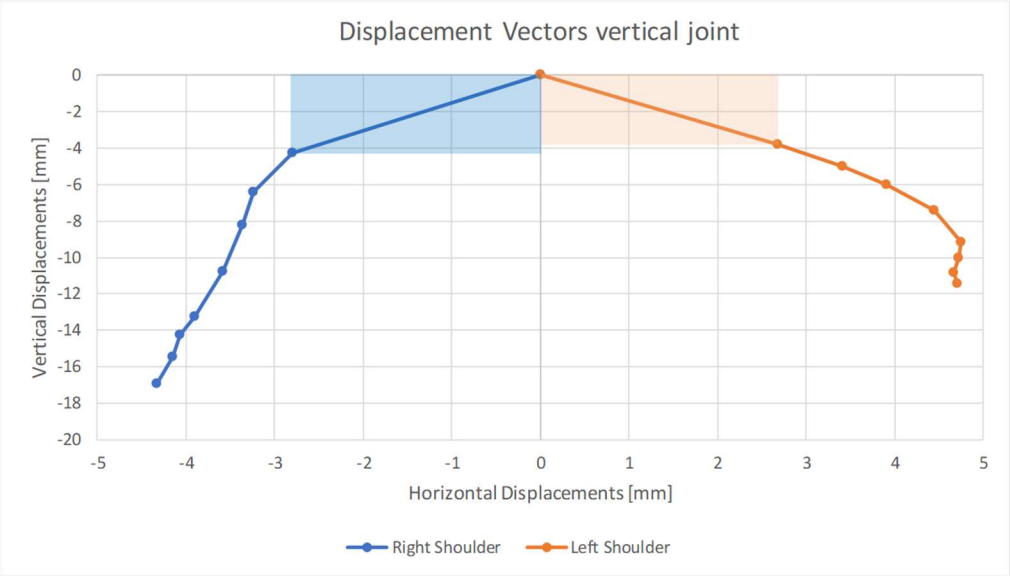

Figure 4.27: Displacement vectors of a model featuring a vertical joint next to the right sidewall

In Figure 4.27, it can be observed that for the chosen parameters, the kink at the right shoulder already occurs between 1m distance and 3m distance to the face. The location of the kink is influenced by the distance o of the joint to the cavity and the strength parameters of the joint.

Here, also there becomes a kink visible in displacement vector at the left shoulder. This can be related to continuous plastification occurring at the left sidewall, reaching the left shoulder at some point as the distance of the face increases as shown in Figure 4.28.

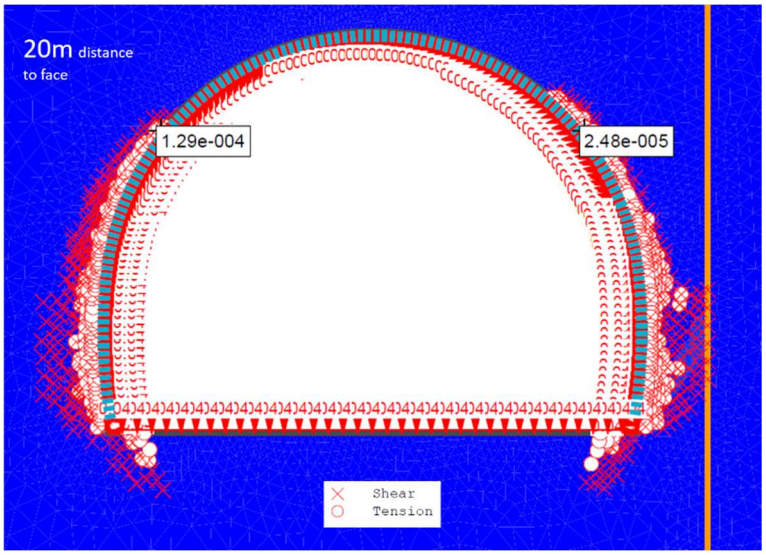

Figure 4.28: Plastification reaching left shoulder at 20m distance to face

In contrast to the results of the previous model, in this model there is no sign of plastification in the area of the right shoulder at the same time as the mechanism provoking the kink in

the displacement vector becomes active. The results of the model simulating the vertical joint as sole anisotropy are depicted in Figure 4.29, Figure 4.30 and Figure 4.31.

Taking a closer look at the plastic deviatoric shear strains in Figure 4.29, Figure 4.30 and Figure 4.31, a different mechanism seems to be observable. A shear band develops, connecting the lower right corner of the cavity with the joint. The formation of this shear band causes a sudden increase in vertical deformations at the right sidewall which results in the kink that can be observed in the results depicted in Figure 4.27.

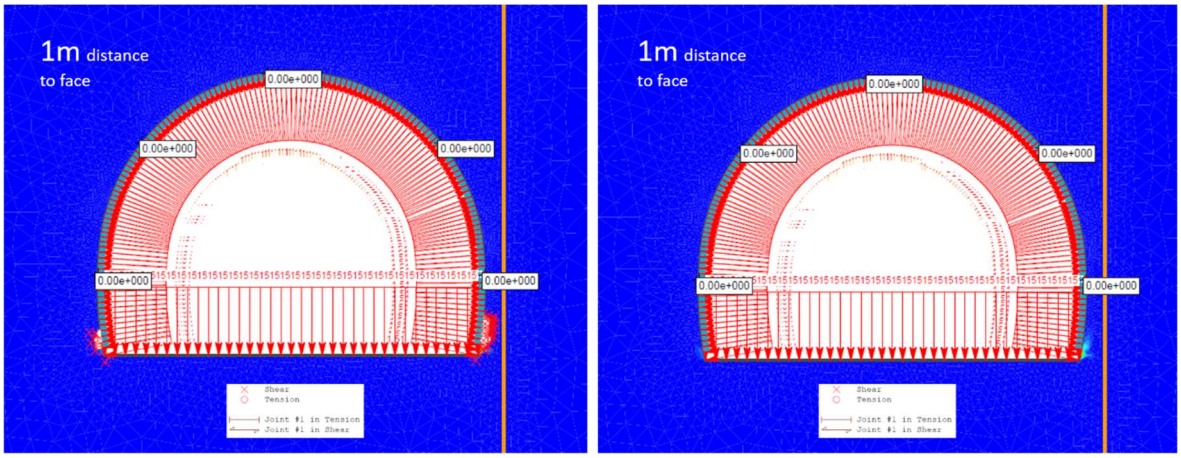

Figure 4.29: 1m distance to face: yielded elements (left), plastic shear strains (right)

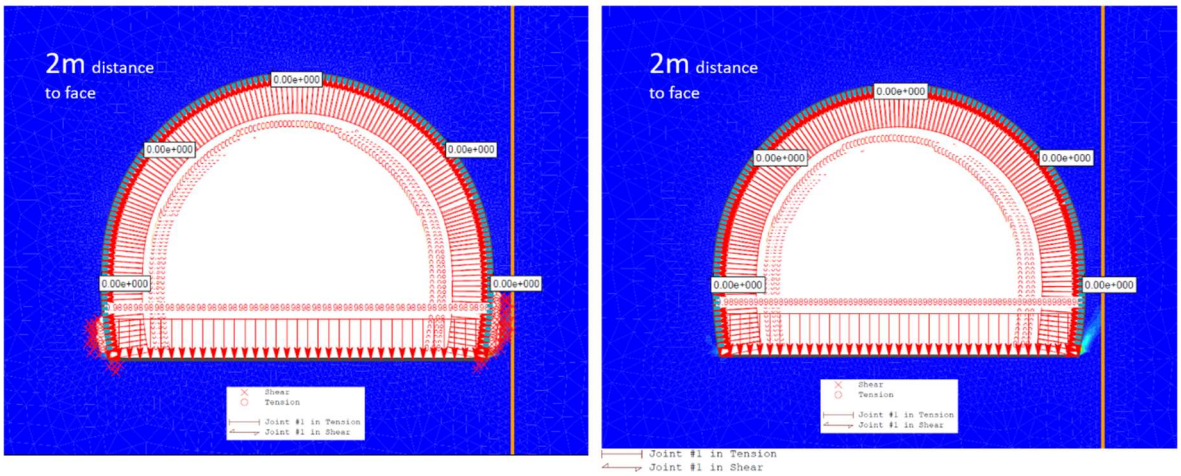

Figure 4.30: 2m distance to face: yielded elements (left), plastic shear strains (right)

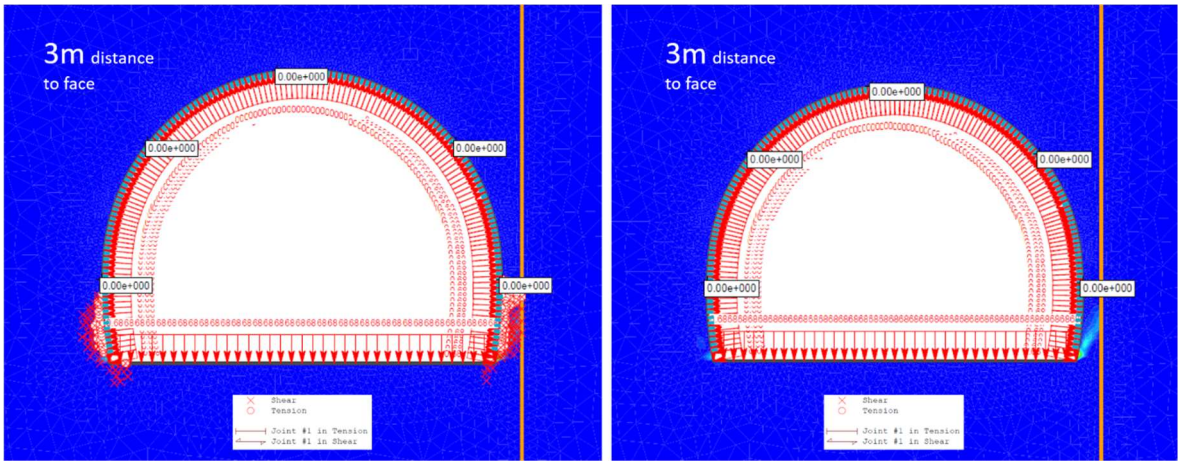

Figure 4.31: 3m distance to face: yielded elements (left), plastic shear strains (right)

4.2.3 Conclusion

In this chapter, the process of the formation of a kink in the displacement vector was analysed. Although it cannot be assured that the mechanisms encountered and described are the only ones that lead to such behaviour, throughout all performed simulations, the two described mechanisms seemed to be consistent. It can be said that the formation of the kink is related to plastic behaviour. In the case of a geomechanically active foliation, this plastification occurs as an activation of the shearing potential of the foliation planes in the vicinity of the right shoulder. For the case of a single discrete fault in the vicinity of the cavity, a shear band develops in the competent rock mass from the base of the excavation to the discontinuity leading to a sudden increase of vertical deformations at the right shoulder. However, in field, the isolated appearance of the described mechanisms does not seem very probable, it will rather be a superposition of those mechanisms described with the activation of further geological features.

4.3 Longitudinal vector rotation of crown point

Further, the behaviour of the displacement vector in longitudinal direction has been assessed for the crown point. The first time that the longitudinal displacement component was used for interpretation was during the construction of the “Inntal” tunnel (14). At this project it was observed that the rotational behaviour of the longitudinal displacement vector is linked to the geological situation ahead of the face. Tunnelling towards an area with different stiffness provokes a rotation of the vector as schematically depicted in Figure 4.32.

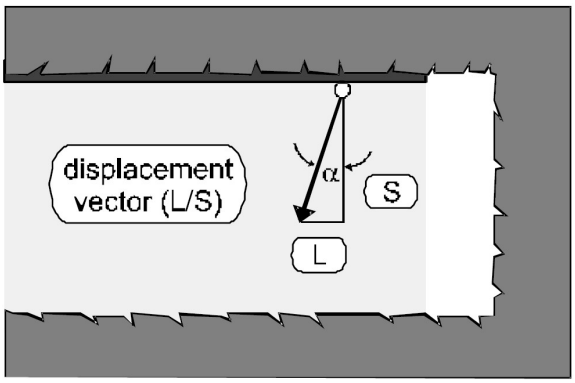

Figure 4.32: Schematic sketch of the displacement vector orientation (L/S); settlement (S) and longitudinal component (L) *(4)*.

Steindorfer (4) later investigated the influence of changing rock mass stiffness on the behaviour of the displacement vector orientation in longitudinal direction.
In this work, the measured longitudinal displacement vector orientations are assessed and compared to the findings of Steindorfer (4). He explains the mechanism determining the orientation of the displacement vector as follows: ”During tunnel excavation displacements are caused by the stress redistribution. When tunnelling in homogeneous ground the rotation of the displacement components and thus the displacement vector orientation, shows a certain value which can be considered as “normal”. Different boundary conditions, like changes in the rock mass structure or in the primary stress situation, influence the stress distribution around the cross section of the tunnel as well as in longitudinal direction ahead of the face, which will show deviations of the vector orientation from the “normal”.” (4)
He performed various 3D numerical analyses and studied the change in stress redistribution as a function of the stress state and the Poisson’s ratio in homogeneous ground conditions, as well as the effect of tunnelling in a rock masses with varying stiffness conditions. He assumed elastic material behaviour and a circular tunnel shape as well as a spherical shape for the face to avoid numerical calculation problems.
He found that the displacement vector generally rotates towards the rock mass with higher stiffness as shown in Figure 4.33 for the case of approaching stiffer material. The rotation

angle of the displacement vector is denoted as α. A positive value for α describes a rotation of the vector against direction of drive, while a negative value for α describes a rotation towards direction of drive.

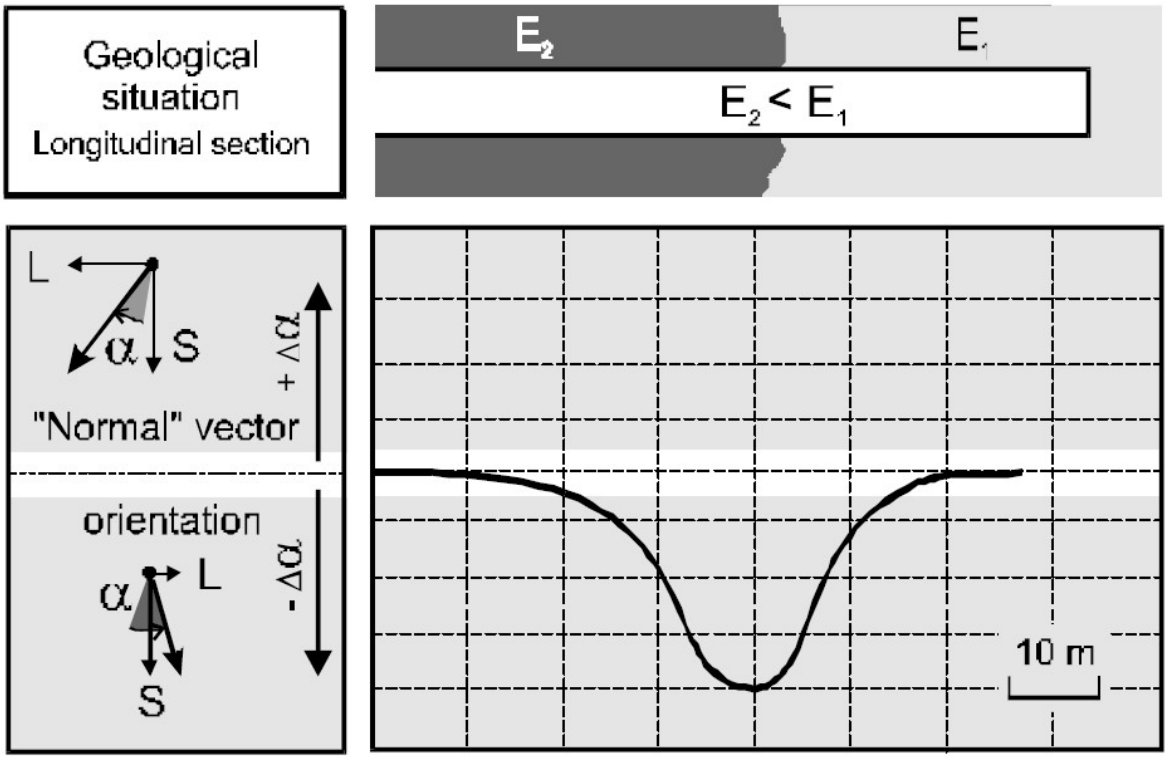

Figure 4.33: "Trend of displacement vector orientation when the excavation approaches and enters the "stiff" rock (schematic)" *(4)*

Note that the graph in Figure 4.33 shows the trend of the deviation from a “normal” vector orientation, not the absolute deviation from the vertical direction.

The longitudinal displacement vector turns against the direction of drive, again towards the stiffer material, as soon as the drive passes the transition from the weak to the stiff rock mass. At some distance to the transition, the displacement vector features again its "normal" orientation.

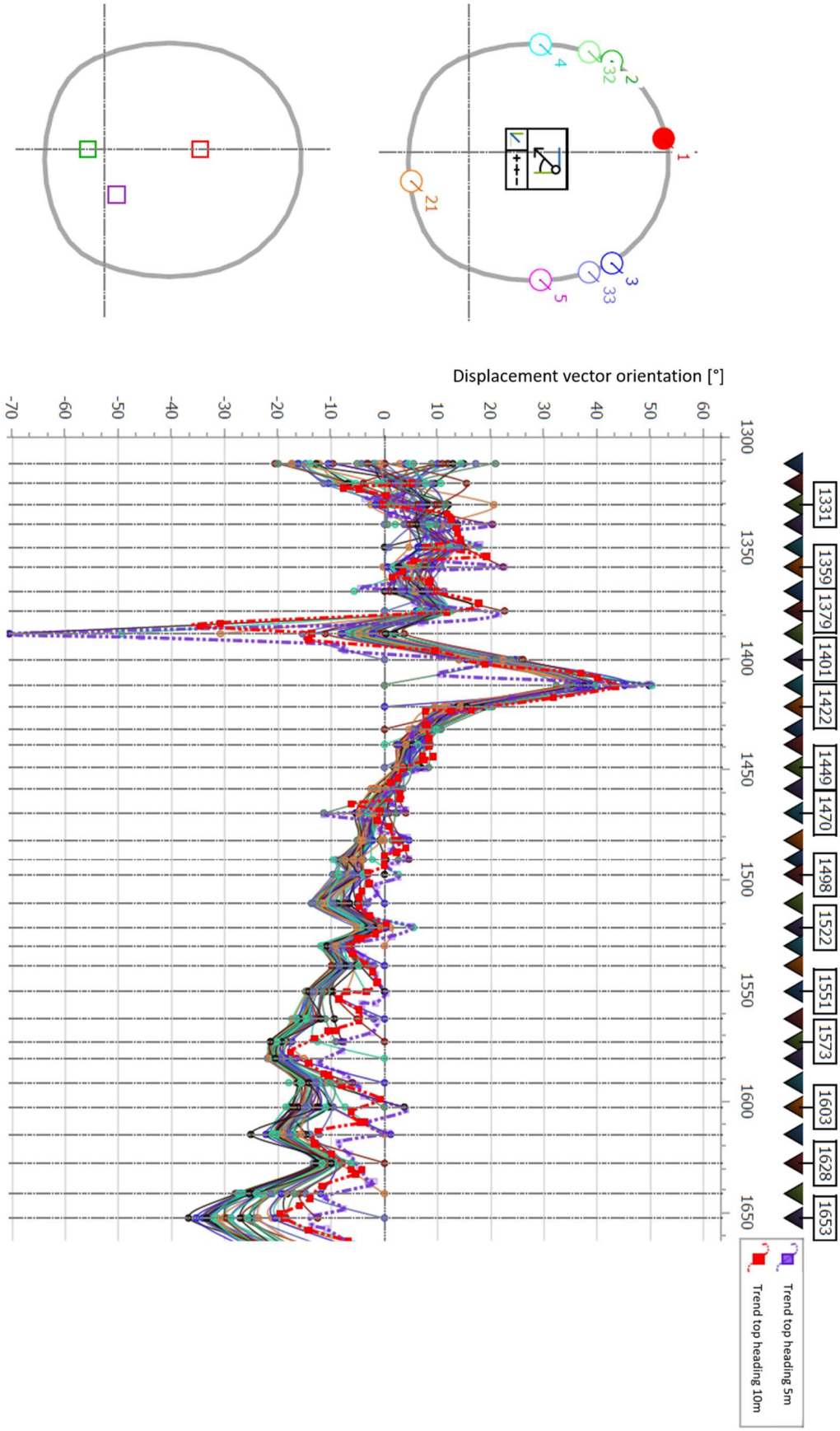

Figure 4.34: Trendlines of the longitudinal displacement vector orientation at the crown *(5)*

In Figure 4.34 the trendlines are shown once 5m behind the face (Trend top heading 5m) and once 10m behind the face (Trend top heading 10m). As it can be seen in Figure 4.34, the determination of a “normal” vector orientation for this case of a heavily disturbed rock mass is not easy. Steindorfer (4) evaluated displacement vectors monitored in tunnels constructed in poor rock and states, that the average angle between the longitudinal displacement vector and the crown settlements (i.e. vertical direction) is between 8° - 12°.

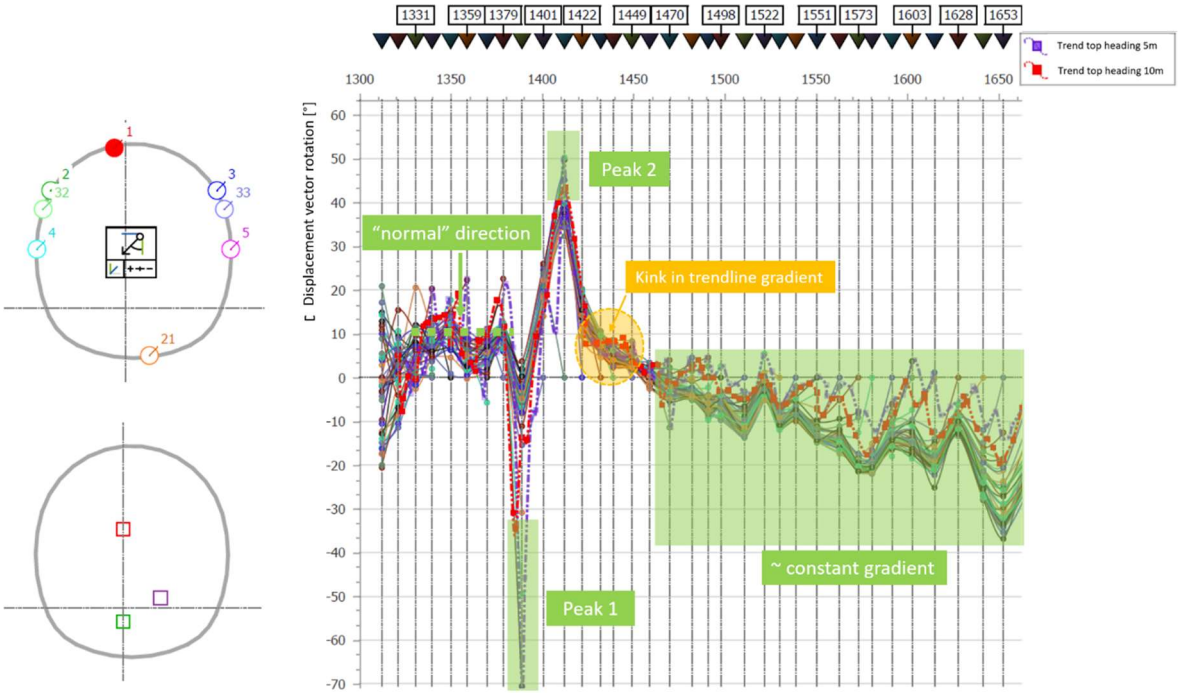

Figure 4.35: Prominent phenomena in the vector orientations in L/S trendline of the crown *(5)*

By looking at the vector orientation between chainage 1340m and 1370m an oscillation around the value of 10° can be seen. Evaluating the rock mass conditions, this vector orientation can be identified to represent the "normal" behaviour (marked with a dashed green line in Figure 4.36). The oscillation can be explained by locally occurring changes in rock strength and stiffness in this area. Furthermore, particularly longitudinal displacements are subjected to a certain measurement inaccuracy. This "normal" behaviour is followed by a pronounced deviation of the vector orientation towards the direction of the drive with a significant peak (approx. 70°; hereinafter called "Peak 1") at chainage 1390m

4.3.1 Assessment of “Peak 1”

To be able to identify the reason for the pronounced rotation of the longitudinal displacement vector resulting in the denoted “Peak 1”, it is necessary to look at the geological situation in more detail. Figure 4.36 shows the geological subhorizontal section of the area between

chainage 1380m and chainage 1400m.

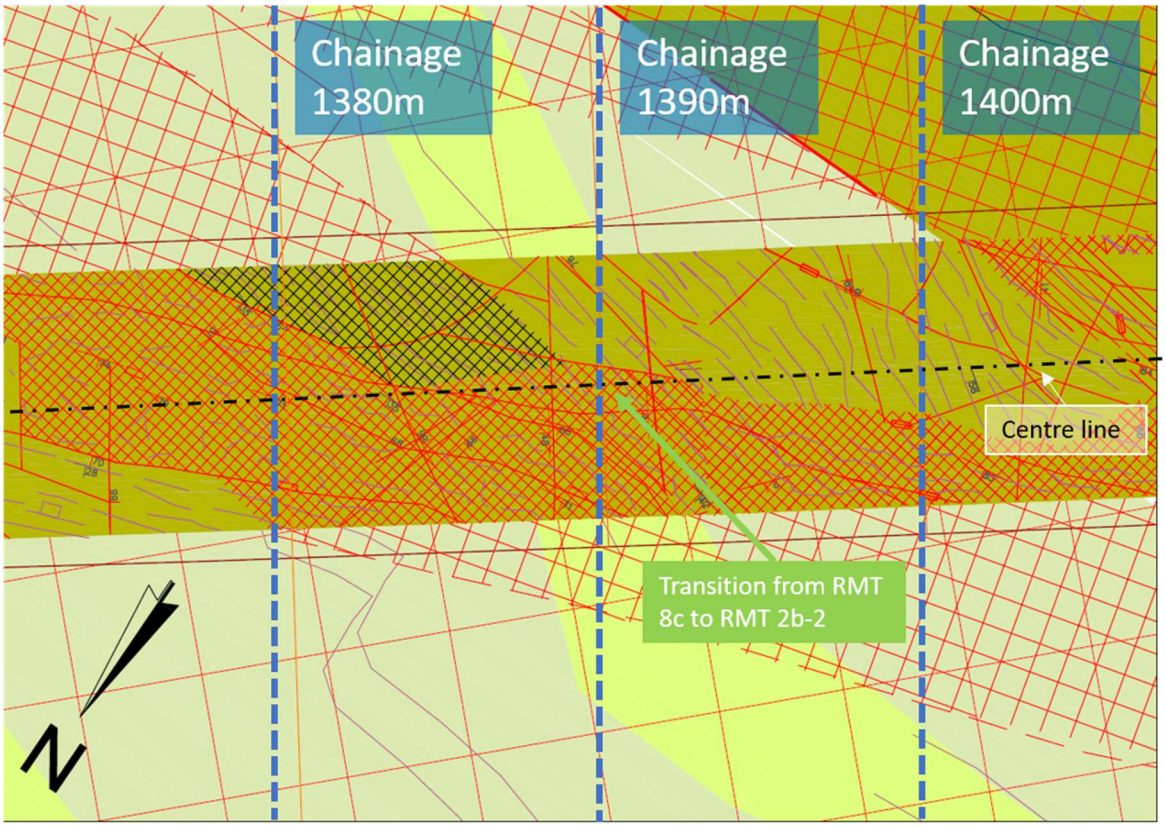

Figure 4.36: Geological subhorizontal section, transition from RMT 8c to RMT 2b-2 at ~ chainage 1390m *(2)*

It becomes evident, that at about chainage 1390m, a transition between the fault material RMT 8c and RMT 2b-2 ($E_1 < E_2$) occurs at the centre of the tunnel. The horizontal section in Figure 4.36 shows the geology at the level of the top heading invert. The fault zone crossing the tunnel from the left to the right between chainage 1370m and 1400m dips with approx. 50° against the direction of the drive. Therefore, the transition from weak to stiffer rock mass at the crown is approx. between chainage 1380m and 1390m. The location of the transition at the crown corresponds with the location of the peak of the vector orientation (see Figure 4.35). The very same development - deviation of the vector orientation in the direction of the drive starts several meters behind the transition (here approx. one diameter) and maximum deviation at the transition - can be observed at numerical simulations (see Figure 4.33).

In Figure 4.33, where the longitudinal section of the geological situation is depicted together with the development of the longitudinal displacement vector orientation, the peak value of the deflection in the trendline also happens at the transition between the rock masses with different stiffnesses.

As well as in the exemplary case in Figure 4.33, the transition at the investigated case

happens from softer to stiffer rock. In both cases, the longitudinal vector orientation rotates in the direction of drive. It can therefore be stated that the phenomenon of “Peak 1” happens in accordance with Steindorfer (4).

4.3.2 Assessment of “Peak 2”

“Peak 2” represents a significant rotation of the longitudinal displacement vector orientation against direction of drive. It occurs at chainage ~1410m and its maximum is approximately 50°. Again, the assessment of “Peak 2” was done analysing the geological situation at the corresponding position.

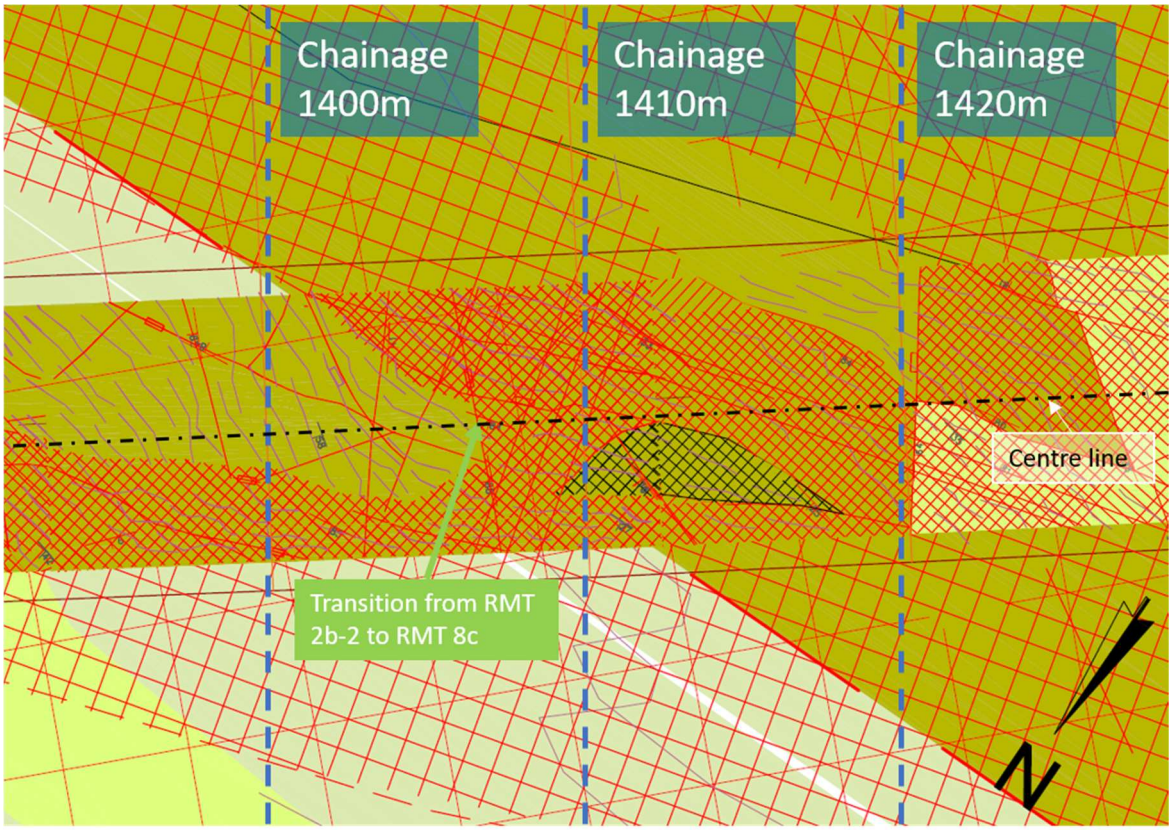

Figure 4.37: Geological subhorizontal section, transition from RMT 2b-2 to RMT 8c at ~ chainage 1405m *(2)*

In Figure 4.37, it becomes evident that a transition from the RMT 2b-2 (higher stiffness) to RMT 8c (lower stiffness) happens close to the peak of the trendline at chainage 1410m. Since the fault zone, which is about to be entered, also dips against the direction of excavation, the transition at the crown is located further in direction of drive than illustrated in the subhorizontal section.

As the rotation of the displacement vector indicates a rotation against the direction of drive at this position it can be stated that also “Peak 2” happens in accordance with the findings

of Steindorfer (4).

4.3.3 Assessment of “Kink in trendline gradient”

Between chainage 1420m and 1450m a kink occurs in the trendline of the longitudinal displacement vector orientation. The trendline plunges from a value of about 50° against the direction of drive at “Peak 2” to a value of about 8° against the direction of drive at chainage 1420m. From chainage 1420m to about chainage 1450m the trendline remains at a value between 8° and 10° against the direction of excavation, corresponding to the value that Steindorfer defined as “normal”.

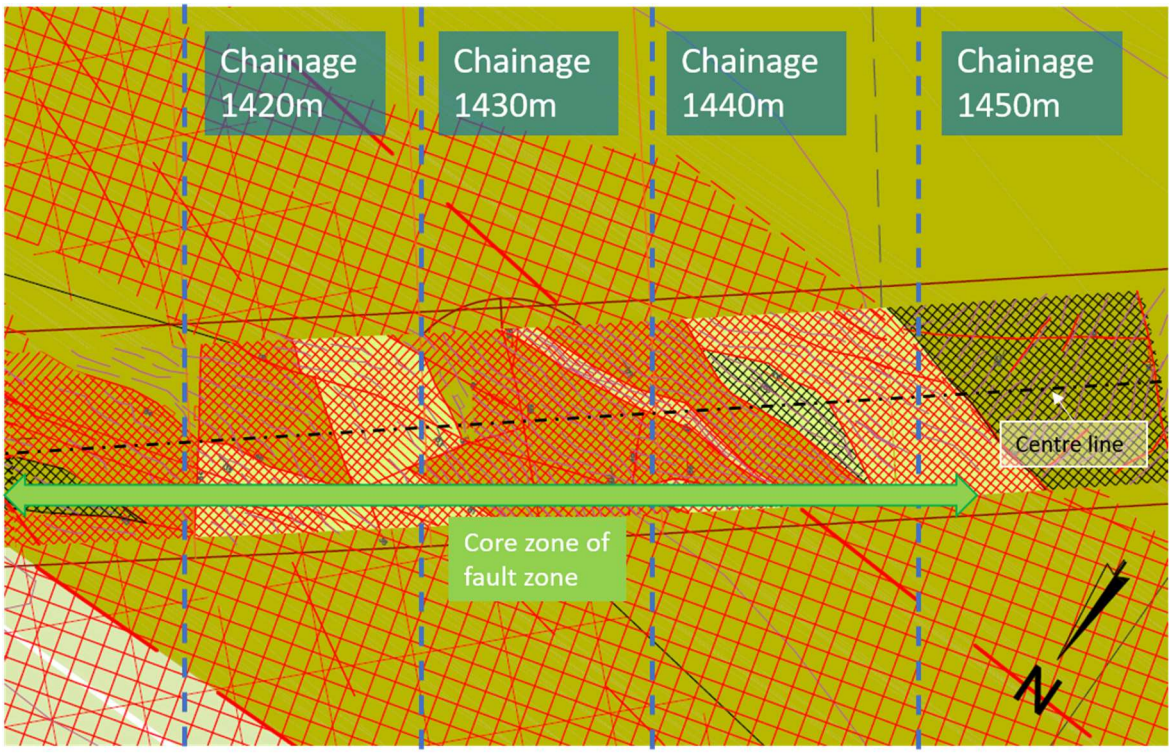

Figure 4.38: Geological subhorizontal section, continuous fault material RMT 8c ~chainage 1420m - ~chainage 1450m *(2)*

By looking at the geological condition in the section between chainage 1420m and chainage 1450m in more detail, it can be found that this section continuously consists of fault material. The “normal” vector orientation between chainage 1420m and chainage 1450m therefore coincides with a constantly disturbed rock mass. This again leads to the conclusion that the findings of Steindorfer, who stated that the “normal” longitudinal vector orientation in a poor rock mass amounts to 8° to 12° ((4) p. 36) is applicable to describe the encountered phenomenon of the kink in the trendline gradient.

4.3.4 Assessment of “constant Gradient”

Steindorfer (4) states that the vector should rotate in direction of drive, when stiffer rock mass is ahead of the face. Once the stiffer rock mass is entered, the vector should begin to rotate back to its normal orientation.

As highlighted in Figure 4.35, the vector is constantly rotating towards the direction of drive for about 200m from chainage 1450m to chainage 1650m in the discussed case. Following the theory according to Steindorfer (4) this would indicate a constant increase of stiffness throughout the section from chainage 1450m to chainage 1650m. To find a suitable explanation for the constant gradient between chainage 1450m and chainage 1650m, first the uniaxial, compressive rock strength distribution throughout this section has been analysed. The data for this has been taken from the face documentations available throughout this section. Since the value for the uniaxial, compressive rock strength is obtained by the geologist and dependent on his subjective interpretation, a categorisation in five steps was made: <1 MPa, 1-5 MPa, 5-25 MPa, 25-50 MPa and 50-100 MPa (2).

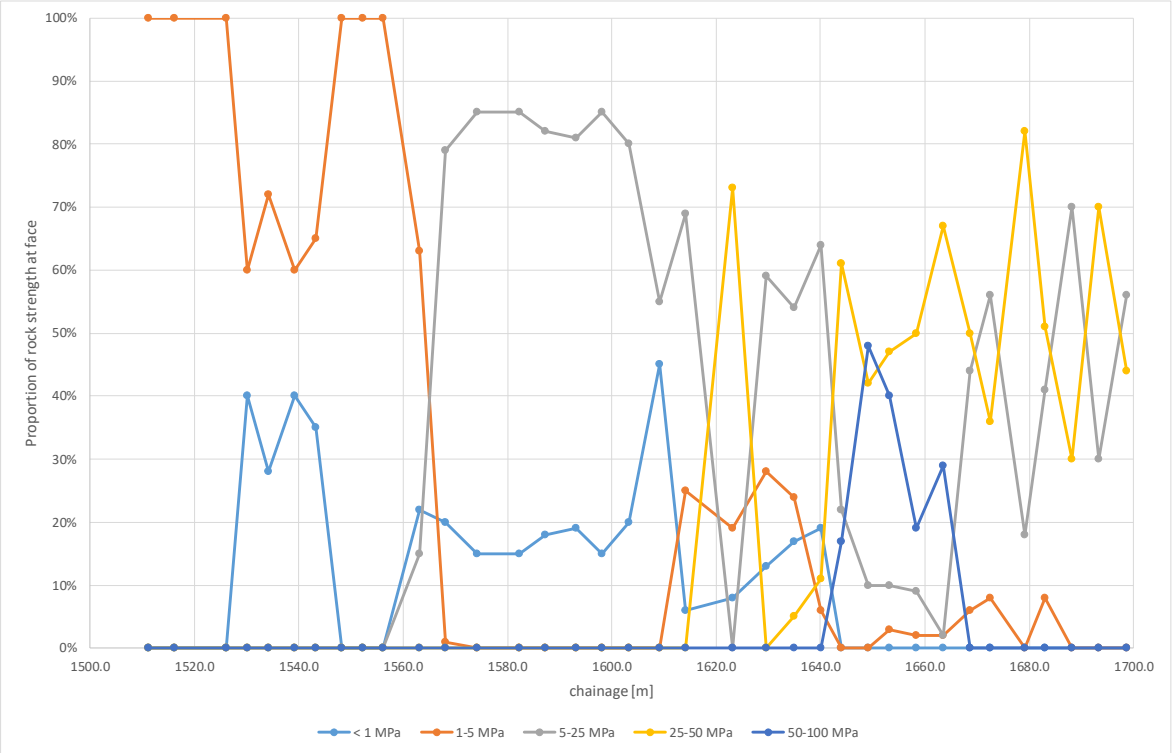

Figure 4.39: Distribution of rock strength throughout the section chainage 1510m - chainage 1700m

As it can be seen in Figure 4.39, the rock strength measured qualitatively at the face is continuously increasing throughout the observed section. Assuming that the rock strength is proportional to the stiffness of the rock mass, this would give a possible explanation for the continuous vector rotation towards the face. A relatively continuous rock strength was

encountered between chainage 1570m and chainage 1600m. In this range the vector rotates back towards “normal” direction, before it turns again towards the face as the rock strength is again improving at chainage 1610m.

Further, Leber (15) investigated the influence of the primary stress state on the vector orientation by performing and assessing 3D numerical models. They generated arbitrarily orientated three-dimensional primary stress fields and investigated the effects on the displacement vectors during tunnel advance. A best-fit plane has been calculated to the deformations in a cross section. The normal vector of this plane was compared to the principal stress vector of the primary stress state to identify a general pattern. It was found that the normal vector of the best-fit plane always rotated towards the direction of the highest principal stress of the primary stress state. Although the normal vector rotation of the best-fit plane does not give an insight on the total displacement at each position, it does show a general behaviour. The displacement vectors turn towards direction of the highest primary stress direction.

Further, a case study has been performed on the “Hinterberg” fault zone. This fault zone was interbedded between two blocks of more competent rock mass. Following the assumption of the arching effect depicted in Figure 4.40, the highest principal stress of the primary stress field should point against the direction drive when the excavation enters the fault zone.

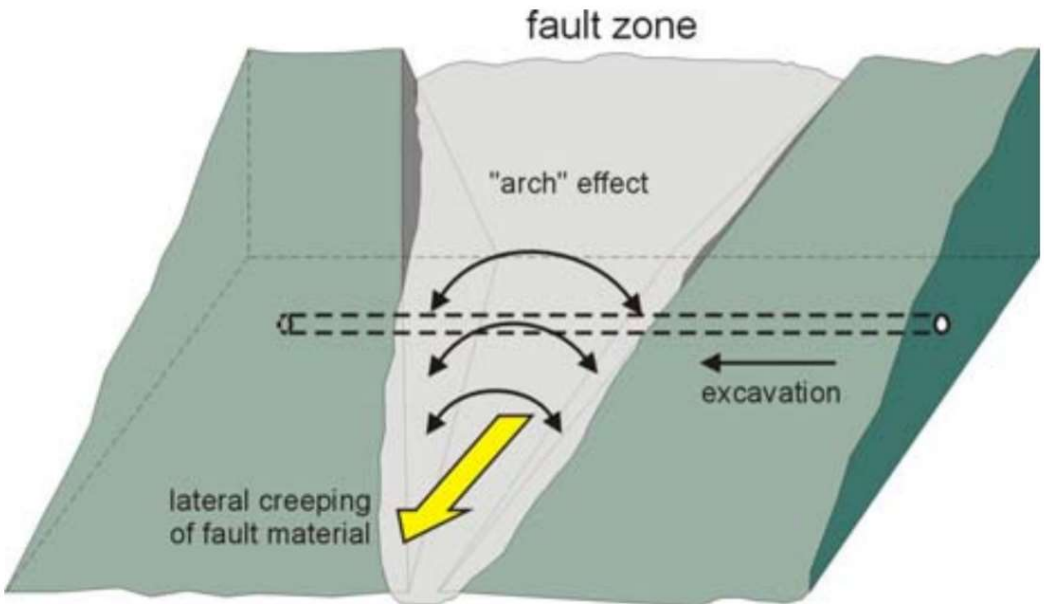

Figure 4.40: "Hinterberg" fault zone wedged between to massive block bodies *(16)*

This primary principal stress direction of the primary stress field should then continuously rotate towards the direction of drive, as the major principal stress direction also rotates with increasing distance from the transition zone between the relatively competent rock mass

and the fault zone as schematically depicted in Figure 4.40. Analogical to the situation entering the fault zone, the major principal stress direction of the primary stress field should point in direction of tunnelling. Consequently, these changes should be visible in the vector orientation. By looking at the L/S trendline of the crown point (Figure 4.41) generated with the displacements measured 15m behind the face, it becomes evident that the vector orientation continuously rotates in direction of drive. The extent of the trendline diagram in the figure below matches the tunnelled distance trough the fault zone.

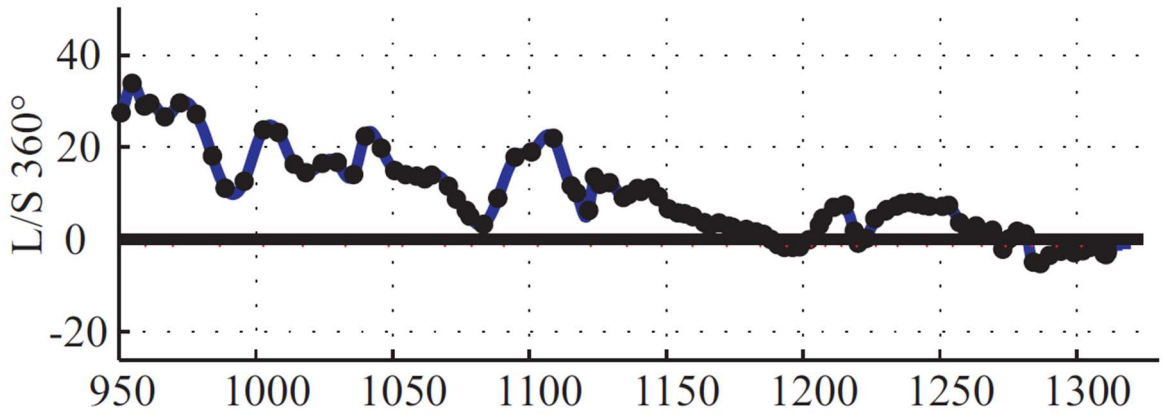

Figure 4.41: Trendline of the vector orientation (L/S) on the crown 15m behind the face *(15)*

Comparing the L/S trendline in Figure 4.41 to the L/S trendline of the currently investigated case (Figure 4.34) it becomes evident, that both trendlines show the same general behaviour. That the constant gradient of the L/S diagram addressed in this chapter is provoked by a rotation of direction of the major principal stress in the primary stress field is therefore considered very probable.

4.3.5 Conclusion

Finally, it can be stated that findings of Steindorfer generally apply for the observed section. When a stiffer rock mass is approached, the displacement vectors tend to rotate towards the direction of drive and analogical they tend to rotate against direction of drive when a softer rock mass is approached.

Comparing the L/S trendline of the crown for the “Hinterberg” fault zone with the section “constant gradient” of the investigated case and relating it to the findings of Leber (15) it seems plausible to assume that the constant gradient in the L/S trendline observed between chainage 1450m and 1650m is also provoked by a change in the primary stress conditions. The origin of this changing stress direction needs to be analysed in further investigative work.

It can be said that the findings of Steindorfer (4) applied in the current case for locally occurring changes in the rock mass stiffness ahead of the face. At the same time, it should be bared in mind, that the overall displacement vector behaviour can be further influenced more globally by effects such as described in the work of Leber (15).

5 Summary

At chainage 1350m a system behaviour occurred, that did not entirely correspond to the provided geological information. By building a 3D numerical model and assessing the generated results, the conclusion has been drawn that a zone of disintegrated rock became active and that this zone extends further to an ESE direction.

By finding correlations between the geological setting and cross sections containing a kink in the displacement vector at either the left or the right shoulder and by implementing those geological settings in a 2D FE model it was possible to link the formation of the kink to a plastic material response. This was achieved for the case where only foliation was considered as anisotropy in the rock mass as well as for the case where a vertical fault close to the cavity was simulated.

It was further found that the displacement data interpretation technique of Steindorfer (4) was applicable to the strongly anisotropic geology in the area of the “Haltestelle Eichberg” fault system. Especially local changes in the rock mass stiffness became clearly evident in the L/S trendlines.

The work of Leber (15) points out that the primary stress field, especially the direction of the major principal primary stress, affects the orientation of the longitudinal displacement vectors in a more global form. Such a situation has become evident in the L/S diagram of the herein investigated case between chainage 1450m and chainage 1650m where the vector turned continuously towards the direction of drive.

This work has shown that the system behaviour in even complex geological conditions can be attributed to its underlying mechanisms by analysing and superposing simple numerical models and using state of the art displacement data interpretation techniques. Knowledge of the cause - effect relation is crucial for the design of an effective tunnel support.

A recommendation for further investigations would be to determine the origin of this rotational behaviour of the vector and if a rotation of the primary stress field can be explained at the same location by putting the tunnel alignment into context with the surrounding topography and by assessing the fault zone architecture of the corresponding location.

Bibliography

1. **Planungsgemeinschaft-Semmering-Basistunnel.** *Internal design documents.*

2. —. *Geological documentation.*

3. **Austrian Society For Geomechanics.** *Geotechnical Monitoring in Conventional Tunnelling.* s.l. : ÖGG, 2014.

4. **Steindorfer, A.** *Short Term Prediction of Rock Mass Behaviour in Tunneling by Advanced Analysis of Displacement Monitoring Data.* s.l. : PhD Thesis at the Institute of Rock Mechanics and Tunnelling of Graz University of Technology, 1997.

5. **Planungsgemeinschaft-Semmering-Basistunnel.** *Displacement monitoring data.*

6. **Davila-Mendez, J. M.** *Displacement Analysis in Layered Rock Masses.* Graz : PhD Thesis at the Institute of Rock Mechanics and Tunnelling of the Graz University of Technology, 2016.

7. **Rocscience Inc.** *RS³ v. 2.0: General Purpose Finite Element Analysis.* Toronto : s.n., 2016.

8. **Goricki, A. et al.** The Influence of Discontinuity Orientation on the Behaviour of Tunnels. *Felsbau.* 23, 2005, Bd. 5.

9. **Inc., Rocscience.** *Phase 2 v. 9.025: Finite Element Anlaysis for Rock and Soil Applications.* Toronto : s.n., 2017.

10. **Fairhurst, C. & Carranza Torres, C.** *Application of the Convergence Confinement Method of Tunnel Design to Rock Masses That Satisfy the Hoek-Brown Failure Criterion.* s.l. : Tunneling and Underground Space Technology, 2000.

11. **Chern, J.C.** *An empirical safety criterion for tunnel construction.* Taipei : s.n., 1998.

12. **Pilgerstorfer, T.** *Prediction of displacement developement using closed form solutions.* Graz : Master's Thesis at the Institute of Rock Mechanics and Tunneling of the Graz University of Technology, 2008.

13. **Arwanitakis, M. & Feder, G.** Zur Gebirgsmechanik ausbruchsnaher Bereiche tiefliegender Hohlraumbauten (unter zentralsymmetrischer Belastung). *Berg- und Hüttenmännische Monatshefte.* Jahrgang 121, 1976, Bd. Heft 4.

14. **Schubert, W.** Erfahrungen bei der Durchörterung einer Großstörung beim Inntaltunnel. *Felsbau.* 11, 1993, Bd. 4.

15. **Leber, C. et al.** *Influence of the primary stress state on the displacement characteristic.* Graz : Technical University of Graz.

16. **Schubert, W. & Riedmüller, G.** Geotechnische Nachlese eines Verbruchs - Erkenntnisse und Impulse. *Mitteilungsheft des Instituts für Bodenmechanik und Grundbau TU-Graz .* Heft 13, S. 59 - 68, 1995.